REVIEW ARTICLE

Upright, Weight-bearing, Dynamic-kinetic Magnetic Resonance Imaging of the Spine — Review of the First Clinical Results

JR Jinkins,[1] JS Dworkin,[2] CA Green,[2] JF Greenhalgh,[2] M Gianni,[2] M Gelbien,[2]
RB Wolf,[2] J Damadian,[2] RV Damadian[2]

[1]Department of Radiological Sciences, Medical College of Pennsylvania-Hahnemann, Drexel University, Philadelphia, Pennsylvania, and [2]Fonar Corporation, Melville, New York, USA

ABSTRACT

Magnetic resonance imaging has, until recently, been limited to scans with patients in the recumbent position. However, a new fully open magnetic resonance imaging unit has been configured to allow upright, partially upright, and recumbent imaging, enabling weight-bearing positional evaluation of the spinal column during various dynamic-kinetic manoeuvres for patients with degenerative conditions of the spine. In a prospective non-statistical analysis of cervical or lumbar imaging examinations, all studies were performed on a whole body magnetic resonance imaging system. The system operates at 0.6 T using an electromagnet with a horizontal field, transverse to the longitudinal axis of the patient's body. The unit was configured with a top/front-open design, incorporating a patient-scanning table with tilt, translation, and elevation functions. The unique motorised patient handling system developed for the scanner allows for vertical (upright, weight bearing) and horizontal (recumbent) positioning of all patients. The top/front-open construction also allows for dynamic-kinetic flexion and extension manoeuvres of the spine. Patterns of bony and soft tissue change occurring among recumbent and upright neutral positions, and dynamic-kinetic acquisitions were sought. Depending on the specific underlying pathological degenerative condition, significant alterations observed on positional and dynamic-kinetic magnetic resonance imaging that were either more or less pronounced than on recumbent magnetic resonance imaging included fluctuating anterior and posterior disc herniations, hypermobile spinal instability, central spinal canal and spinal neural foramen stenosis, and general sagittal spinal contour changes. No patients had claustrophobia that resulted in termination of the examination. The potential relative benefits of upright, weight-bearing, dynamic-kinetic spinal imaging over that of recumbent magnetic resonance imaging include the revelation of occult disease dependent on true axial loading, the unmasking of kinetic-dependent disease, and the ability to scan the patient in a position clinically relevant to the signs and symptoms. This imaging technique demonstrated a low claustrophobic potential and yielded relatively high-resolution images with little motion/magnetic susceptibility/chemical shift artifacts. Overall, it was found that recumbent imaging underestimated the maximum degree of degenerative spinal pathology and missed its dynamic nature altogether — factors that are optimally revealed with positional/dynamic-kinetic magnetic resonance imaging.

Key Words: Kinetics, Magnetic resonance imaging, Spine, Weight bearing

INTRODUCTION

Magnetic resonance imaging (MRI) using commercial systems has, until recently, been limited to acquiring scans with patients in the recumbent position. It is a logical observation that the human condition is subject to the effects of gravity in positions other than that of recumbency.[1] In addition, it is clear that patients experience signs and symptoms in dynamic manoeuvres of the spinal column other than the recumbent one. For this reason, a new fully open MRI unit was configured to allow upright, partially upright, and recumbent imaging. This also enables partial or full weight bearing and simultaneous kinetic manoeuvres of the patient's whole body or any body part. The

objective was to facilitate imaging of the body in any position of normal stress, across the limits of range of motion, and in the specific position of the patient's clinical syndrome. Under optimised conditions it was hoped that a specific imaging abnormality might be linked with the specific position or kinetic manoeuvre that produced the clinical syndrome. In this way imaging findings could potentially be meaningfully linked to patients' signs and symptoms. Furthermore, it was anticipated that radiologically occult but possibly clinically relevant weight bearing- and/or kinetic-dependent disease not visible on the recumbent examination would be unmasked by the positional-dynamic imaging technique.[2] This report represents a clinical review of the first observations acquired with this versatile imaging unit.

TECHNIQUE

The initial study involved a prospective, non-statistical analysis of cervical or lumbar MRI examinations. All examinations were performed on a recently introduced full body MRI system (Stand-Up™ MRI, Fonar Corporation, Melville, USA) [Figure 1]. The system operates at 0.6 T using an electromagnet with a horizontal field, transverse to the axis of the patient's body. Depending upon spinal level, all examinations were acquired with either a cervical or lumbar solenoidal radiofrequency receiver coil. The MRI unit was configured with a top-open design, incorporating a patient-scanning table with tilt, translation, and elevation functions. The unique MRI-compatible, motorised patient handling system developed for the scanner allows vertical (upright, weight bearing) and horizontal (recumbent) positioning of all patients. The top-open construction also allows dynamic-kinetic flexion and extension manoeuvres of the spine.

Sagittal lumbar/cervical T1- (TR: 680; TE: 17; NEX: 3; ETL: 3) weighted fast spin echo imaging (T1FSEWI), sagittal lumbar/cervical T2- (4000, 140-160, 2, 13-15)

Figure 1. Various patient/table configurations of the Stand-Up™ magnetic resonance imaging unit. (a) Patient in the standing position (standing-neutral pMRI); (b) patient in the recumbent position (rMRI); (c) patient in the Trendelenberg position (negative angled pMRI); (d) patient in seated-upright position (seated-neutral pMRI); (e) patient in cervical flexion-extension manoeuvres (kMRI); (f) patient in lumbar flexion-extension manoeuvres (kMRI).

weighted fast spin echo imaging (T2FSEWI), axial lumbar T1WI (600, 20, 2) or T1FSEWI (800, 17, 3, 3), axial cervical gradient recalled echo T2*-weighted (620-730, 22, 2) [T2*GREWI] were performed for all cervical/lumbar studies. For all patients, recumbent neutral, upright neutral, upright flexion, and upright extension imaging was performed. The patients were seated for the upright cervical examinations and for the neutral upright lumbar acquisitions, and were placed in the standing position for the lumbar kinetic studies.

Patterns of bony and soft tissue change occurring among recumbent neutral (rMRI) and upright neutral positions (pMRI), and dynamic-kinetic acquisitions (kMRI: upright flexion-extension) were sought (Table 1) Specifically, degenerative spinal disease including focal intervertebral disc herniations, spinal stenosis involving the central spinal canal and spinal neural foramina, and hypermobile spinal instability were compared with other visibly normal segmental spinal levels among the rMRI, the pMRI, and kMRI acquisitions

Table 1. Patient positioning-related variations of magnetic resonance imaging (MRI).

*R*ecumbent MRI: rMRI:
- Supine, recumbent imaging

*P*ositional MRI: pMRI:
- Imaging in varying angular positions of longitudinal axis of body

*K*inetic MRI: kMRI:
- Imaging during dynamic-kinetic somatic manoeuvres (flexion, extension, rotation, lateral bending)

Table 2. Dynamic spinal alterations.

Bony structures:
- Intersegmental relationships
- Range of motion
- Spinal contour

Intervertebral discs:
- Disc height
- Disc margin

Ligaments:
- Ligamentotactic effects
- Ligamentopathic effects

Perispinal muscles

Neural tissue
- Spinal cord
- Spinal nerve roots: ventral and dorsal
- Cauda equina

Table 3. 'Telescoping' of spinal column in degenerative disease.

Intersegmental settling:
- Disc collapse
- Posterior spinal facet (zygapophyseal) joint subluxation

Annulus fibrosus redundancy

Ligamentous redundancy

Meningeal redundancy

Neural redundancy

(Tables 2, 3, 4, 5, 6, and 7). Focal disc herniations were defined as localised protrusions of intervertebral disc material that encompassed less that 25% of the total disc periphery in the axial plane. Central spinal stenosis was defined as generalised narrowing of the central spinal canal in the axial and/or sagittal plane relative to that of other spinal levels. Spinal neural foramen narrowing was defined as general narrowing of the neural foramina as determined from sagittal acquisitions relative to that of other segmental spinal levels. Hypermobile spinal instability was defined as relative mobility between adjacent spinal segments compared with other spinal levels that in turn demonstrated virtually no intersegmental motion. Generally speaking, degenerative disc disease was defined as both intrinsic discal MRI signal loss as well as morphological alteration to include a reduction in superoinferior dimensional disc space height. Alterations in sagittal spinal curvature were also noted between the neutral rMRI and pMRI acquisitions (Table 8). Finally, notation was made as to whether or not the patient was referred in part because of an inability to undergo a prior MRI due to subjective feelings of claustrophobia attempted in a 'closed' MRI unit. As this was to be a general review of first clinical results, no statistical analysis was sought.

Table 4. Types of intersegmental spinal motion.

- Eumobility: normal motion
- Hypermobility: increased motion in the X, Y, Z planes
- Hypomobility: decreased motion

Table 5. Positional fluctuation in spinal ligaments and discs (p/kMRI).

Ligamentotactic effects:
- Intact spinal ligamentous structures
- Contained bulging peripheral disc material
- Inclusion of disc material within disc space when ligaments are tensed
- Further protrusion of disc material into perispinal space when ligaments are relaxed

Table 6. Dysfunctional intersegmental motion (DIM).

- DIM is a form of intersegmental hypermobile instability
- DIM results from intersegmental degenerative disease
- DIM engenders progressive, generalised accelerated intersegmental degeneration
- Mechanism of accelerated spinal degeneration: uncontrolled chronic-repetitive autotrauma

Table 7. Translational hypermobile instability of the spinal column.

Ligamentopathic alterations: ligamentous stretching/rupture
- Mobile translational antero- and retrolisthesis (X-plane)
- Mobile latero- and rotolisthesis (Z and Y-planes)
- Dynamic overextension of spinal range(s) of motion (X, Y, Z planes)

Table 8. Types of upright postural spinal curvature.

Normal curvature
- Cervical: lordotic
- Thoracic: kyphotic
- Lumbar: lordotic

Exaggerated curvature
- Hyperlordosis
- Hyperkyphosis

Loss of sagittal spinal curvature ('straight spine')
- Hypolordosis
- Hypokyphosis

Coronal plane scoliosis (direction of convex spinal curve)
- Leftward: levoscoliosis
- Rightward: dextroscoliosis
- Serpentine: serpentine scoliosis

The neutral upright imaging studies (neutral-pMRI) demonstrated the assumption by the patient of the true postural sagittal cervical or lumbar lordotic spinal curvature existing in the patient at the time of the MRI examination, a feature that was partially or completely lost on the neutral rMRI (Figures 2 and 3). In other words, this relative postural sagittal spinal curvature correction phenomenon was manifested by a change from a straight or even reversed lordotic curvature on rMRI to a more lordotic one on pMRI. Increasing severity of focal posterior disc herniation on the neutral-pMRI compared with the rMRI was noted (Figure 3),
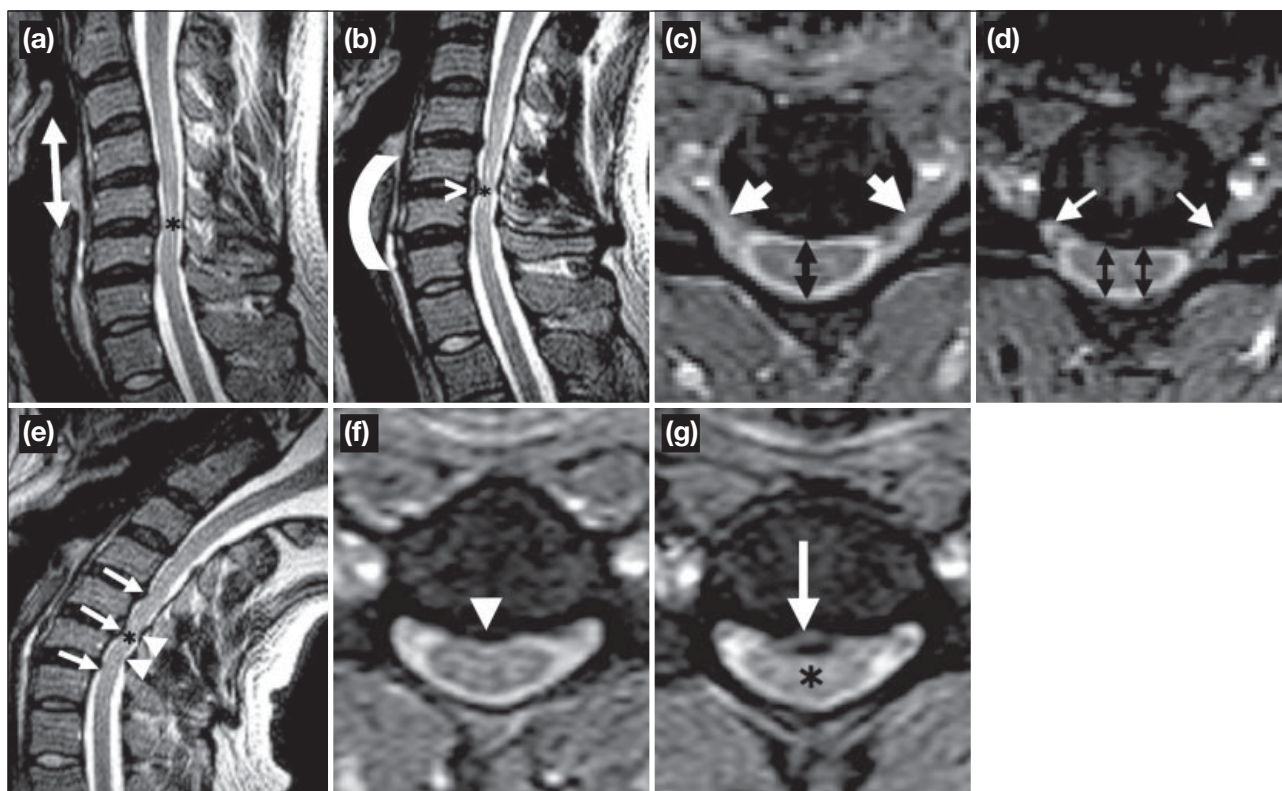

Figure 2. Sagittal cervical spinal curvature correction; unmasking of central spinal stenosis; occult herniated intervertebral disc (all images from the same patient). (a) Recumbent midline sagittal T2-weighted fast spin echo magnetic resonance image (rMRI) shows straightening and partial reversal of the sagittal spinal curvature of the cervical spine (double headed arrow). Minor posterior disc bulges/protrusions are present at multiple levels, but the spinal cord (asterisk) is not compressed. (b) Upright-neutral midline sagittal T2-weighted fast spin echo magnetic resonance image (pMRI) shows partial restoration of the true sagittal postural cervical curvature upon neutral-upright positioning (curved line). Note the relative increase in the posterior disc protrusion at the C5-6 level (arrowhead) and encroachment on the spinal cord (asterisk) compared with the recumbent image in Figure 2a. (c) Recumbent axial T2*-weighted gradient recalled echo magnetic resonance image (rMRI) through the C4-5 level shows patent neural foramina bilaterally (single headed arrows), and mild stenosis of the central spinal canal (double headed arrow). (d) Upright-neutral axial T2*-weighted gradient recalled echo magnetic resonance image (pMRI) through the C4-5 level shows bilateral narrowing of the neural foramina (single headed arrows). Note also the narrowing of the central spinal canal (double-headed arrows) relative to the recumbent study (Figure 2c), and the compression of the underlying spinal cord (relative antero-posterior flattening of the spinal cord compared with the recumbent image [Figure 2c]). (e) Upright-extension midline sagittal T2-weighted fast spin echo magnetic resonance image (extension kMRI) shows further posterior protrusion of the intervertebral discs at multiple levels (arrows) and anterior infolding of the posterior spinal ligaments (arrowheads), resulting in overall worsening of the stenosis of the central spinal canal. Note the impingement (compression) of the underlying spinal cord (asterisk) by these encroaching spinal soft tissue elements. (f) Recumbent axial T2*-weighted gradient recalled echo magnetic resonance image (rMRI) at the C5-6 disc level shows posterior paradiscal osteophyte formation (arrowhead) extending into the anterior aspect of the central spinal canal. Note that the cervical spinal cord is atrophic, but there is a rim of cerebrospinal fluid hyperintensity entirely surrounding the cord. (g) Upright-extension axial T2*-weighted gradient recalled echo magnetic resonance image (extension kMRI) revealing (extension-related) focal posterior disc herniation (arrow). Note the overall increased stenosis of the central spinal canal and the compression-indentation of the underlying cervical spinal cord (asterisk).
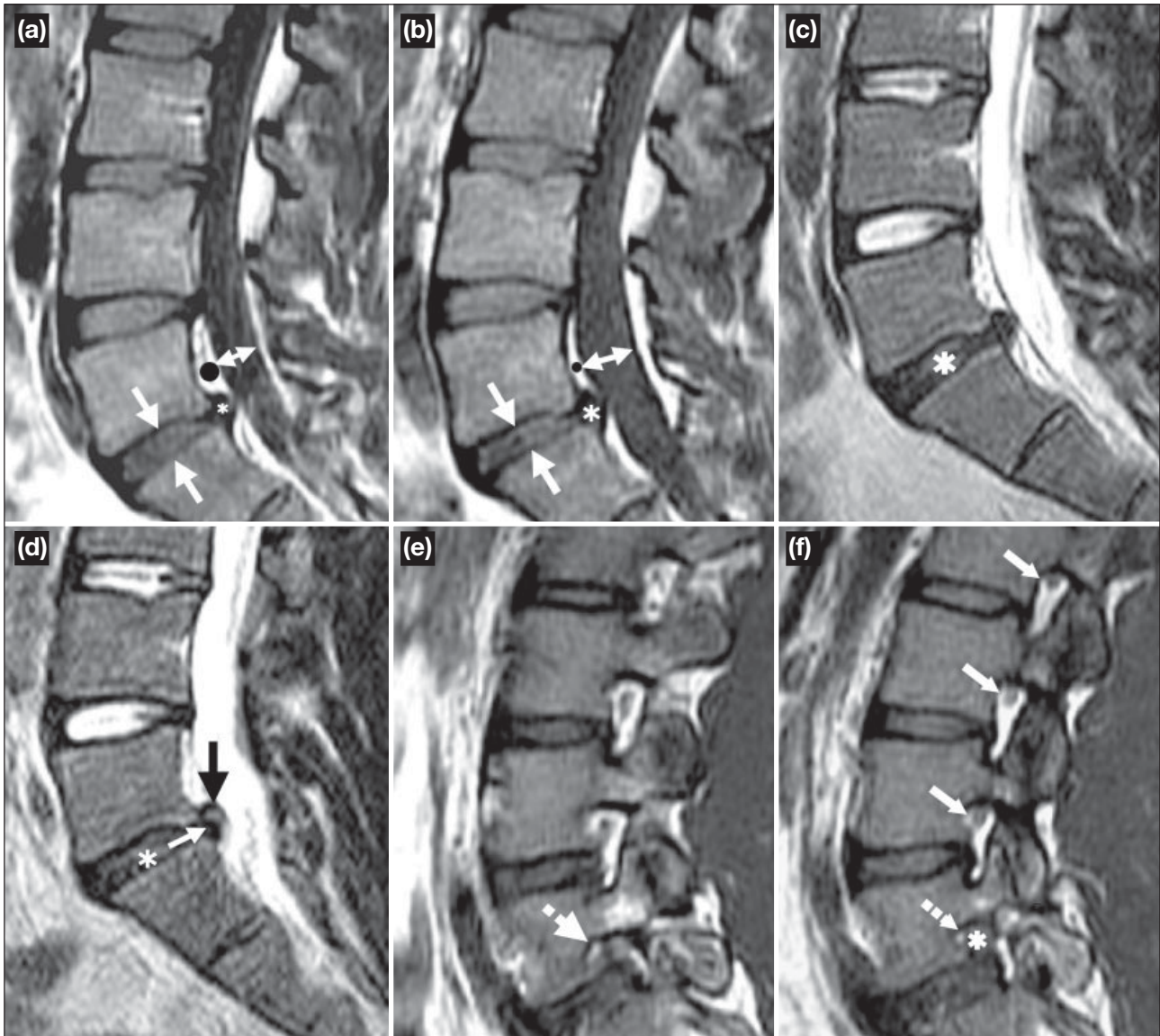
Figure 3. Effects of gravity on the intervertebral disc, thecal sac, and spinal neural foramina; true sagittal postural lumbosacral curvature.
(a) Recumbent midline sagittal T1-weighted fast spin echo magnetic resonance image (rMRI) shows a focal disc herniation at L5/S1 (asterisk) and mild narrowing of the superoinferior disc height at this level (single headed arrows). Note also the anteroposterior dimension of the thecal sac (double headed arrow), and the size of the anterior epidural space (dot) at the L4 level. (b) Upright-neutral (standing) midline sagittal T1-weighted fast spin echo magnetic resonance image (pMRI) shows minor further narrowing of the height of the L5/S1 intervertebral disc (single headed arrows) and enlargement of the posterior protrusion of the disc herniation at this level (asterisk) [see also Figure 3a]. Also note the generalised expansion of the thecal sac (double headed arrow) because of gravity-related hydrostatic cerebro-spinal fluid pressure increases, and the consonant decrease in the dimensions of the anterior epidural space (dot: theoretically caused by a reduction in volume of the anterior epidural venous plexus). Note that the upright-standing spine now assumes the true sagittal postural curvature on this image, compared with the recumbent image (Figure 3a). (c) Recumbent midline sagittal T2-weighted fast spin echo magnetic resonance image (rMRI) shows the posterior disc herniation at L5-S1 (asterisk). (d) Upright-neutral midline sagittal T2-weighted fast spin echo magnetic resonance image (pMRI) shows further narrowing of the L5-S1 intervertebral disc (asterisk; see Figure 3c) and a new component to the posterior disc herniation (black arrow) resulting in overall enlargement of the size of the herniation (compare with Figure 3c). Apparently, this observed enlargement is caused by intradiscal fluid (water) and/or disc material exiting via an unvisualised posterior radial annular tear (white arrow) into the epidural space. Since fluids and semifluids (water; nucleus pulposis) are non-compressible, the reduction in size of the disc volume makes it necessary for the intradiscal fluids/semifluids to evacuate via some route, a radial annular tear being the most likely pathway. Some degree of radial peripheral disc bulging may also contribute to this phenomenon. (e) Recumbent midline parasagittal T1-weighted fast spin echo magnetic resonance image (rMRI) on the patient's left side shows narrowing of the L5/S1 spinal neural foramen (dashed arrow) as a result of posterior disc protrusion, intervertebral disc space narrowing and paradiscal osteo-phyte formation. (f) Upright-neutral midline parasagittal T1-weighted fast spin echo magnetic resonance image (pMRI) on the patient's left side reveals minor generalised narrowing of all of the spinal neural foramina (solid arrows), including the L5/S1 level (dashed arrow) [see recumbent examination, Figure 3e]. At some point in this stenotic process, the exiting neurovascular bundle (asterisk) will undergo compression and may become symptomatic.

and was even worse in degree on extension-kMRI (Figure 2). These posterior disc herniations were less severe on flexion-kMRI manoeuvres compared with all other acquisitions (Figure 4). Absolute de novo appearance of disc herniation on neutral-pMRI was identified on extension-kMRI acquisitions in some cases compared
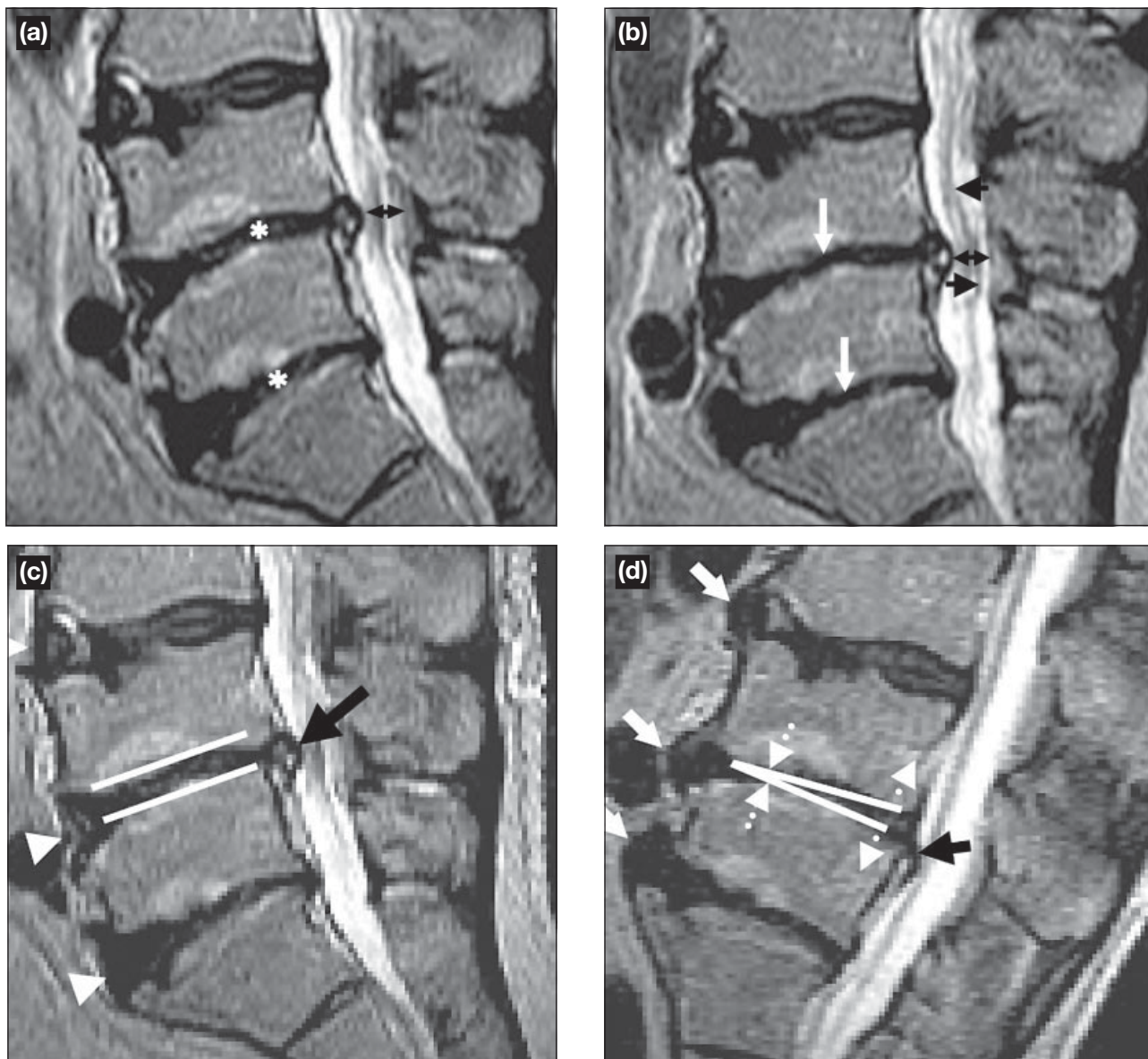

Figure 4. Telescoping of the spinal column; reducing posterior disc herniation; increasing anterior disc protrusions; dysfunctional intersegmental motion. (a) Recumbent mid-line sagittal T2-weighted fast spin echo magnetic resonance image (rMRI) showing degenerative disc disease at all levels, especially severe at L4-5 and the L5-S1 levels (asterisks). A focal posterior disc herniation is noted at the L4-5 level. Note the narrowed (stenotic) anteroposterior dimension of the thecal sac at the L4-5 level (double headed arrow). Also note the diffuse hyperintensity of the interspinous spaces indicating rupture of the interspinous ligaments at multiple levels. (b) Upright-neutral midline sagittal T2-weighted fast spin echo magnetic resonance image (pMRI) revealing further gravity-related narrowing of the intervertebral discs at multiple levels (white arrows) compared with the recumbent examination (rMRI; Figure 4a). This represents telescoping of the spinal column. Note also the minor increase in narrowing of the anteroposterior dimension of the thecal sac (double headed arrow), and the increased redundancy of the nerve roots of the cauda equina (black arrows). (c) Recumbent mid-line sagittal T2-weighted magnetic resonance image showing the relative parallel surfaces of the vertebral end plates at L4-5 (white lines), and the flat surfaces of the anterior aspects of the intervertebral discs at multiple levels (white arrowheads). Note again the posterior disc herniation at the L4-5 level (black arrow). (d) Upright-flexion mid-line T2-weighted fast spin echo magnetic resonance image (kMRI) showing increases in size of the anterior disc protrusions at multiple levels (white solid arrows) and a reduction of the posterior disc herniation at the L4-5 level (black arrow), compared with the r/pMRI studies. Also note the opening up (enlargement) of the posterior aspect and the closing (narrowing) of the anterior aspect of the L4-5 disc space (dashed white arrows), with resulting anterior angulation of the vertebral end plates (white lines). The latter phenomenon represents dysfunctional intersegmental motion. Finally, note the hypersplaying of the spinous processes (with consonant hyperexpansion of the interspinous space[s]), indicating rupture of the interspinous ligament(s).

with rMRI (Figure 2). A reduction of intervertebral disk height was typically noted at levels of disc degeneration (Figures 3 and 4). Increasing severity of central spinal canal stenosis was identified on neutral-pMRI and on extension-kMRI acquisitions compared with rMRI, and was most severe on extension and least severe on flexion-kMRI acquisitions (Figures 2 and 5). Similarly, increasing severity of spinal neural foramen
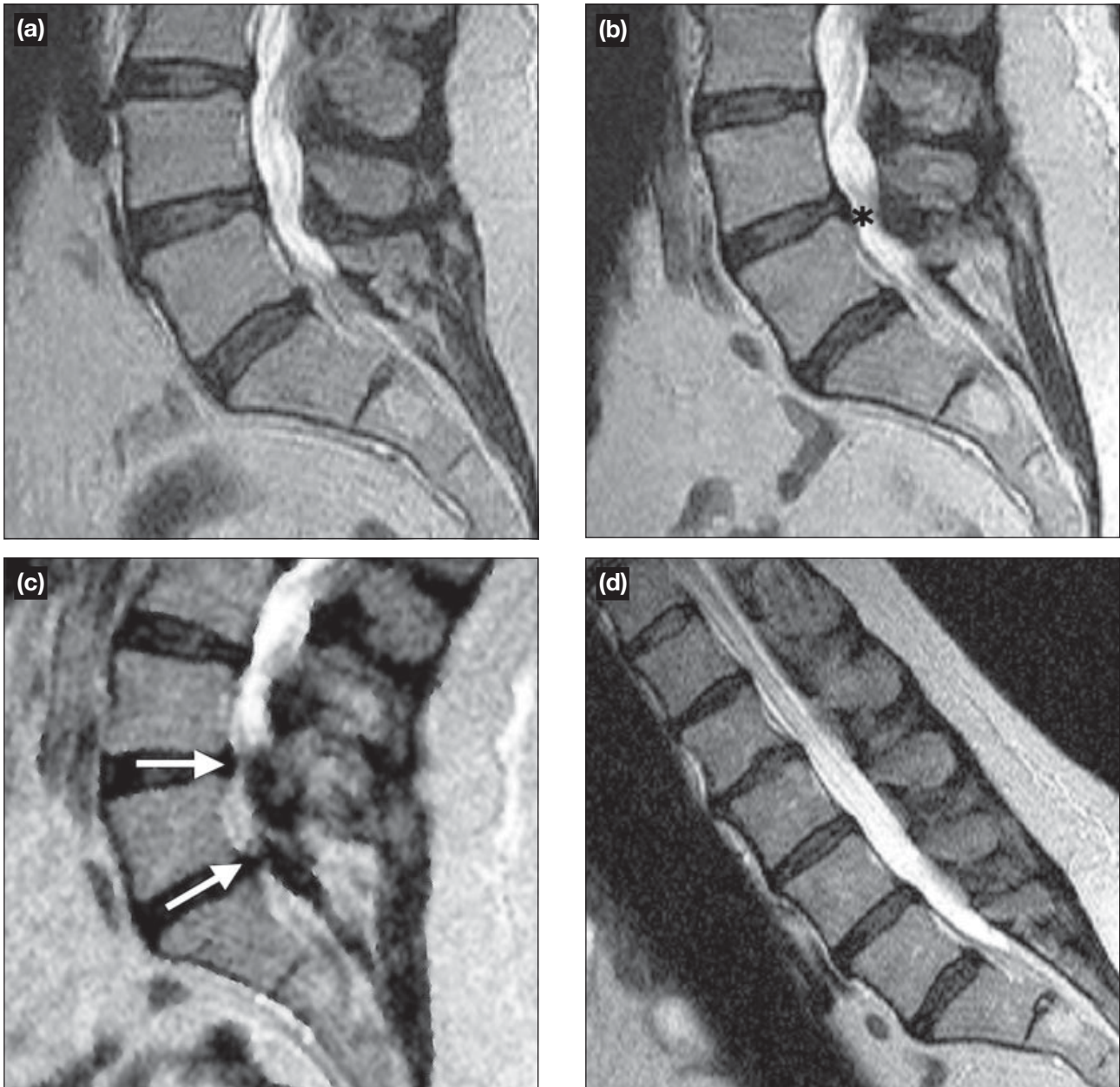

Figure 5. Worsening-reducing central spinal canal stenosis on dynamic-kinetic magnetic resonance image (kMRI); minor translational intersegmental hypermobile instability on dynamic-kinetic magnetic resonance image (kMRI). (a) Recumbent mid-line sagittal T2-weighted fast spin echo magnetic resonance image (rMRI) shows mild, generalised spondylosis and minor generalised narrowing of the central spinal canal. (b) Upright-neutral mid-line sagittal T2-weighted fast spin echo magnetic resonance image (pMRI) shows very minor worsening of the central spinal canal stenosis inferiorly (asterisk) relative to the recumbent image (Figure 5a). Note the assumption by the patient of the true postural sagittal lordotic curvature of the lumbosacral spine compared with the recumbent examination. (c) Upright-extension mid-line sagittal T2-weighted fast spin echo magnetic resonance image (kMRI) reveals severe worsening of the central spinal canal stenosis in the lower lumbar area (arrows; L4-5, L5/S1). This results from a combination of factors, including redundancy of the thecal sac and spinal ligaments and increasing posterior protrusions of the intervertebral discs at L4-5 and L5-S1. (d) Upright-flexion mid-line sagittal T2-weighted fast spin echo magnetic resonance image (kMRI) demonstrates complete reduction of the posterior disc protrusions at the L4-5 and L5-S1 levels, and resolution of the central spinal canal stenosis at these lumbar segments (compare with Figure 5c). Also note that there is minor anterolisthesis at the L2-3 and L4-5 levels compared with the neutral examinations (Figures 5a and 5b), indicating associated mild translational intersegmental hypermobile instability at these levels.

stenosis was identified on neutral-pMRI (Figure 3) compared with rMRI, and was overall most severe on extension and least severe on flexion-kMRI acquisitions (Figure 6). Increasing central spinal canal narrowing with spinal cord compression on extension-kMRI was identified in some cervical examinations (Figure 2) compared with recumbent rMRI, neutral-pMRI, and flexion-kMRI manoeuvres. Translational sagittal plane
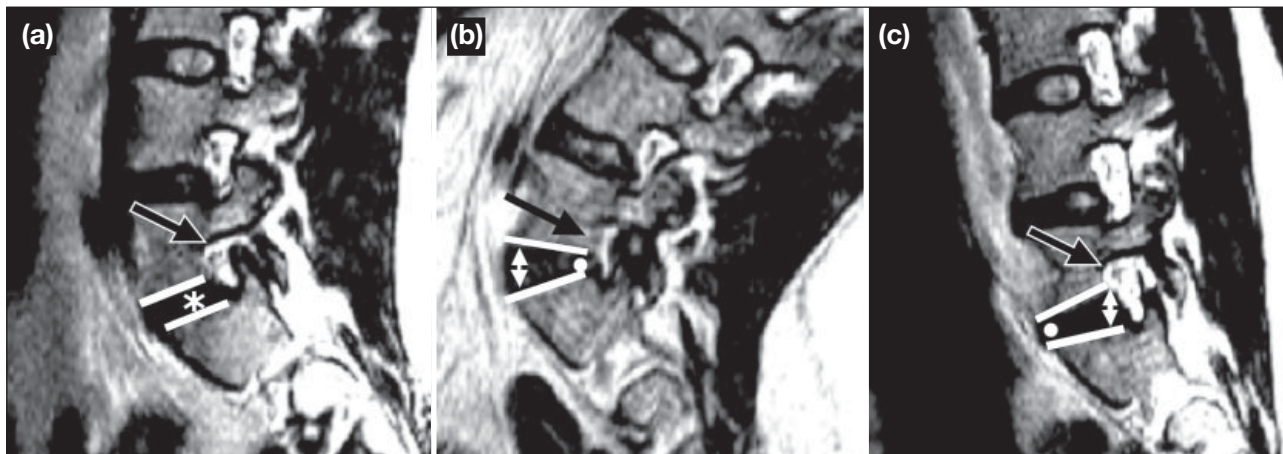

Figure 6. Effects of dynamic-kinetic manoeuvres (kMRI) on spinal neural foramina at levels of degenerated disc disease and theoretical ligamentous laxity (ligamentopathy); dysfunctional intersegmental motion. (a) Recumbent parasagittal T2-weighted fast spin echo magnetic resonance image (rMRI) shows intervertebral disc degeneration at the L5-S1 level (asterisk). Note the mild narrowing of the neural foramen (arrow) at this level (minor foraminal stenosis), and the near parallel surfaces of the vertebral end plates (lines). (b) Upright-extension parasagittal T2-weighted fast spin echo magnetic resonance image (kMRI) reveals further narrowing of the neural foramen at L5-S1 (arrow) relative to the recumbent image (Figure 6a). Note the opening of the anterior aspect of the disc space (double headed arrow), closing of the posterior aspect of the disc space (dot), and resulting posterior angulation of the vertebral endplates (lines). The neural foramina at other levels are minimally narrowed compared with the recumbent image (Figure 6a). (c) Upright-flexion parasagittal T2-weighted fast spin echo magnetic resonance image (kMRI) demonstrates opening of the neural foramen at L5-S1 (arrow), the opening of the posterior aspect of the disc space (double headed arrow), closing of the anterior aspect of the disc space (dot). Note the anterior angulation of the vertebral end plates (lines). Figures 6b and 6c illustrate dysfunctional intersegmental motion in addition to the dynamic changes in the size of the neural foramen at levels of disc degeneration and theoretical ligamentous laxity (ligamentopathy). The neural foramina at other levels are somewhat enlarged compared with the recumbent and the extension images (Figures 6a and 6b).
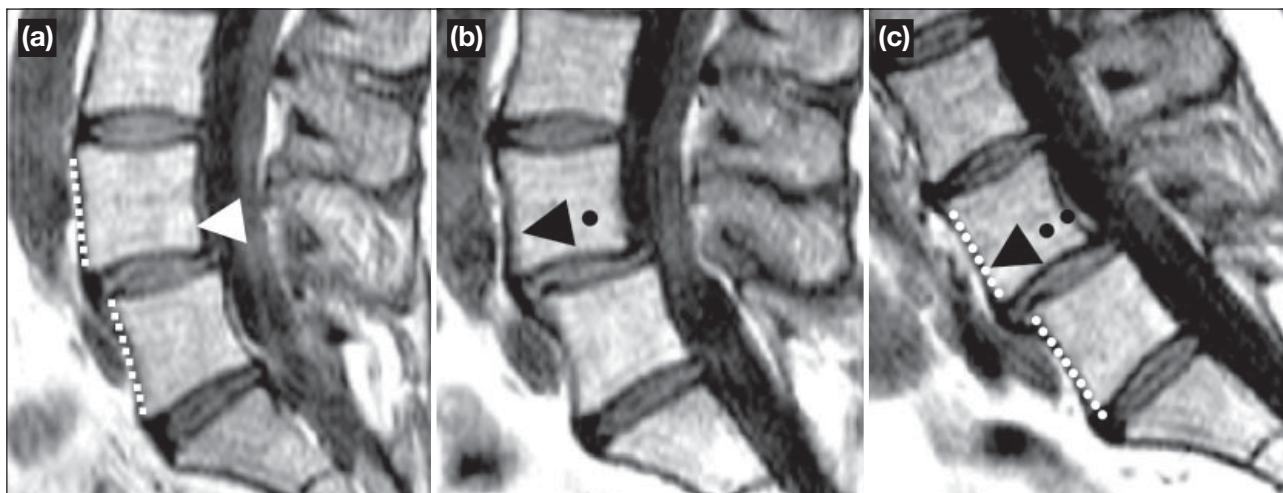

Figure 7. Translational hypermobile spinal instability associated with degenerative anterior spondylolisthesis related in part to theoretical ligamentous laxity (ligamentopathy). (a) Recumbent mid-line sagittal T1-weighted fast spin echo magnetic resonance image (rMRI) shows minor (> grade I) degenerative anterior spondylolisthesis at the L4-5 level (arrowhead). The pars interarticularis was intact on both sides at this level. Note the relationship between the anterior surfaces of the L4 and L5 vertebral bodies (dashed lines). (b) Upright-neutral mid-line sagittal T1-weighted fast spin echo magnetic resonance image (pMRI) reveals minor worsening of the anterior slip of L4 on L5 (dashed arrow) compared with the recumbent examination. (c) Upright-flexion mid-line sagittal T1-weighted fast spin echo magnetic resonance image (kMRI) demonstrates further anterior subluxation of L4 on L5 in flexion (dashed arrow) compared with Figures 7a and 7b. This demonstrates the dynamic translational hypermobile instability sometimes associated with degenerative spondylolisthesis and in part related to ligamentopathy. Note the relationship between the anterior surfaces of the L4 and L5 vertebral bodies (dashed lines), and the difference compared with the recumbent image (Figure 7a).
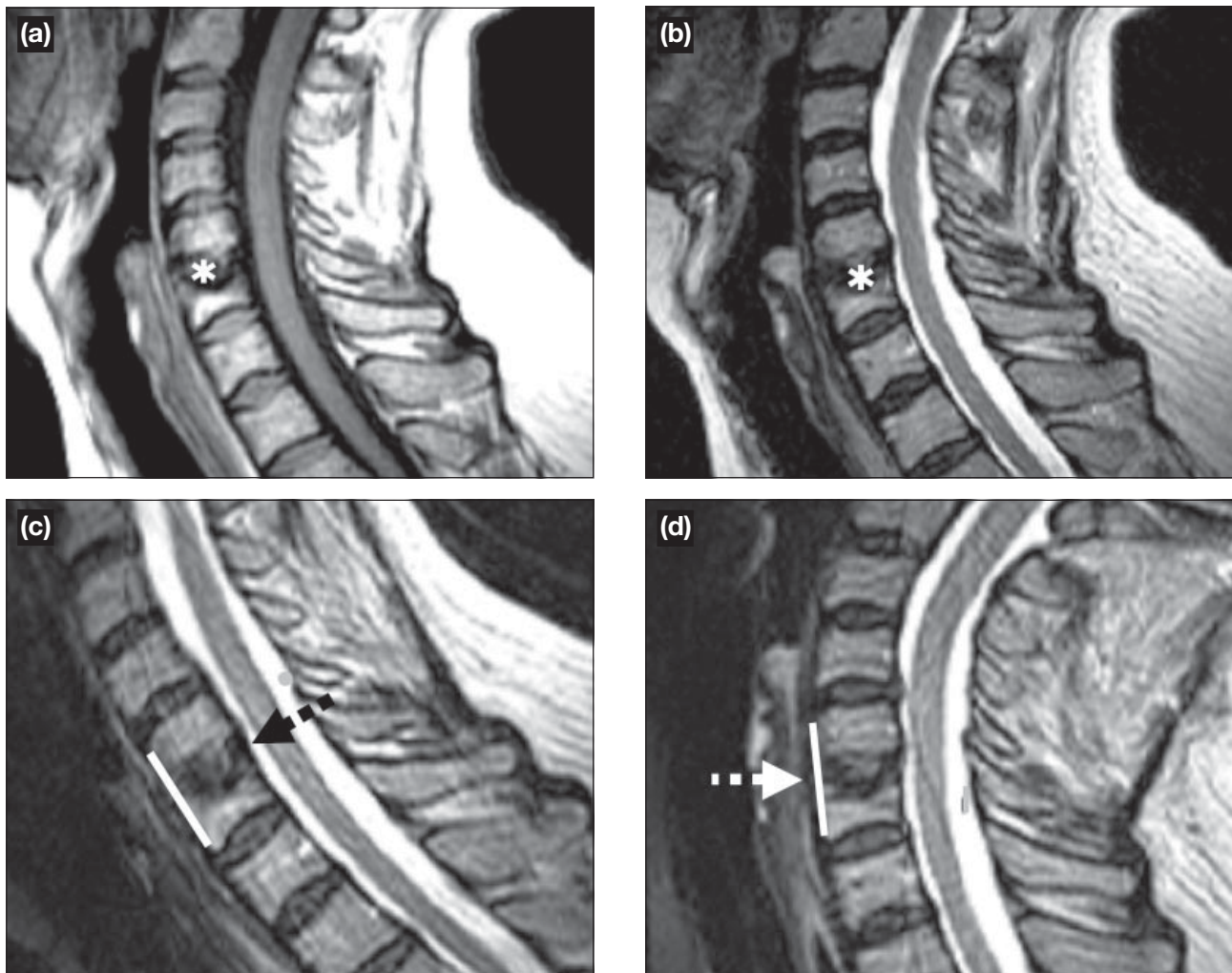
Figure 8. Postoperative intersegmental fusion stability (4 years post-clinically successful interbody bone graft fusion). (a) Upright-neutral mid-line sagittal T1-weighted fast spin echo magnetic resonance image (pMRI) shows the surgical fusion at C5-6 (asterisk); autologous bony dowels were used for the original fusion performed 4 years prior to the current examination. Note the normal bony intersegmental vertebral alignment and normal upright postural sagittal lordotic curvature. (b) Upright-neutral midline sagittal T2-weighted fast spin echo magnetic resonance image (pMRI) again shows the intersegmental fusion (asterisk). Note the good spatial dimensions of the cerebro-spinal fluid surrounding the spinal cord. (c) Upright-flexion (arrow) mid-line sagittal T2-weighted fast spin echo magnetic resonance image (kMRI) shows no intersegmental slippage at, suprajacent to, or subjacent to the surgically fused level (solid line). Note the maintenance of the anteroposterior dimension of the central spinal canal. (d) Upright-extension (arrow) mid-line sagittal T2-weighted fast spin echo magnetic resonance image (kMRI) again reveals no intersegmental hypermobile instability (no intersegmental mobility; solid line) or central spinal canal compromise at any level.

intersegmental hypermobility was identified at some levels associated with degenerative disk disease and minor anterolisthesis of a degenerative nature (Figures 5 and 7). Postoperative spinal stability was identified across levels of prior surgical fusion (Figure 8). No examination was uninterpretable based on patient motion during any portion of the MRI acquisitions. No patient was unable to complete the entire examination due to subjective feelings of claustrophobia.

APPLICATION

Conventional rMRI is theoretically inadequate for a complete and thorough evaluation of the spinal column and its contents. The biomechanics of the human condition includes both weight bearing body position-ing and complex kinetic manoeuvres in 3 dimensions.[3-6] The new MRI unit is intended to address these consider-ations. Both occult weight bearing disease (focal inter-vertebral disc herniations, spinal stenosis, thecal sac volumetric change), and kinetic-dependent disease (disc herniations, spinal stenosis, hypermobile instabil-ity) of a degenerative nature[7-23] have been unmasked by the p/kMRI technique. In addition, a true assessment of the patient's sagittal weight bearing postural spinal curvature is possible on neutral-upright pMRI, there-by enabling better evaluation of whether the loss of
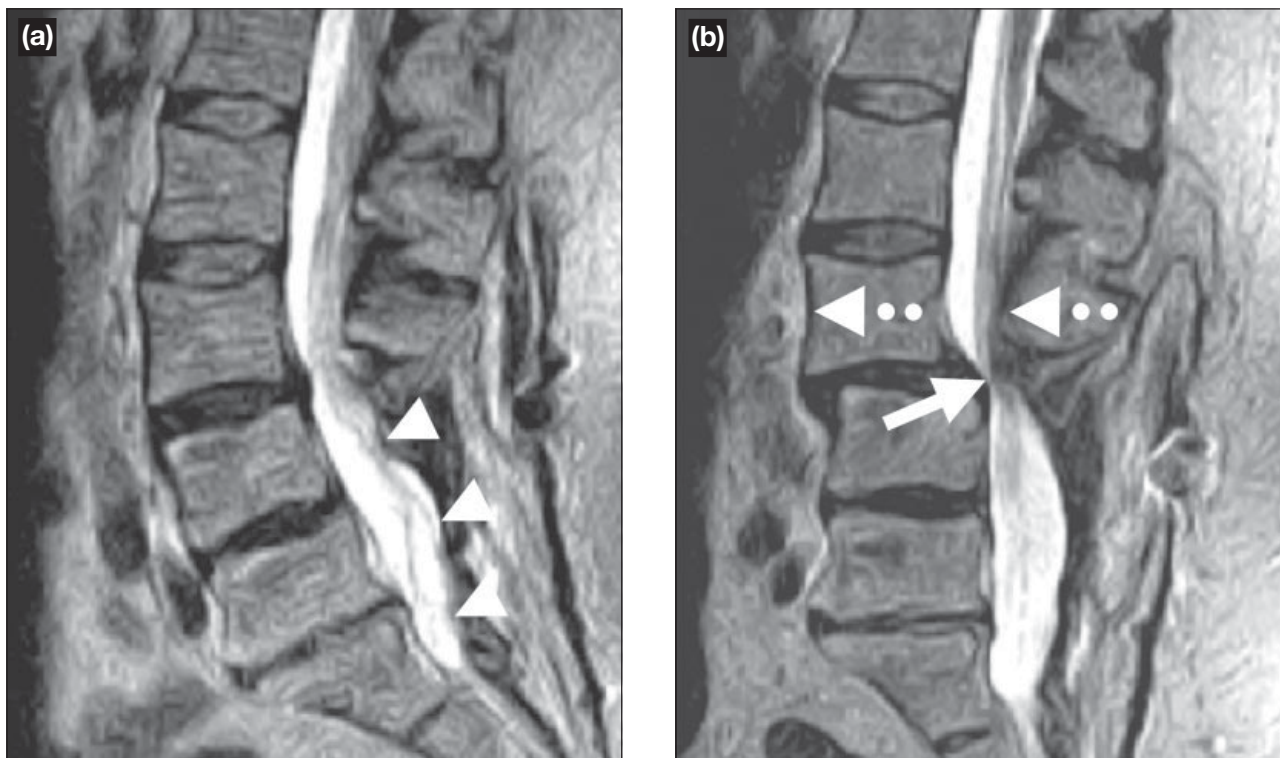
Figure 9. Postoperative intersegmental hypermobile instability at the segment above fusion, 5 years following bilateral fusion (pedicle screws and rods extending between L4-S1) and bilateral laminectomy at the L4-S1 levels. (a) Recumbent midline sagittal T2-weighted fast spin echo magnetic resonance image (rMRI) shows bilateral laminectomy extending from L4-S1 (arrowheads). The patient also had bilateral pedicle screws and rods extending from and to the same levels (not shown). No metallic artifact is present because the surgical materials were composed of titanium. (b) Sagittal-upright-sitting (i.e., partial flexion) mid-lineT2-weighted fast spin echo magnetic resonance image (p/kMRI) demonstrates marked anterior slip of the L3 vertebral body upon the L4 vertebra (dashed arrows). Also note the resultant marked stenosis of the central spinal canal at the L3-4 level (solid arrow), and resultant encroachment of the bony structures of the spine upon the cauda equina. (Case provided courtesy of Dr M Rose.)

curvature is due to patient positioning (rMRI) or as a probable result of somatic perispinal muscular guarding or spasm (Figures 2 and 3). Axial loading and dynamic flexion-extension studies by other researchers have borne out these varied observations out.[24-38]

Non-dynamic upright weight-bearing MRI, or upright-neutral pMRI, shows a phenomenon termed 'telescoping' whereby the levels of generalised intersegmental spinal degeneration show a collapse of the spine into itself (Figure 4).[39] Consequent redundancy of the discal, ligamentous, and meningeal tissues of the spine resulted in increased degrees of central canal and lateral recess spinal stenosis, while craniocaudal shortening of the spine associated with telescoping caused increased degrees of neural foramen stenosis (Figure 3). On occasion, the degree of frank posterior disc herniation was seen to enlarge with upright pMRI (Figure 3). This latter finding would seem to be an important observation, obviously improving the qualitative nature of the analysis in relevant cases of disc herniation. Finally, upright-neutral imaging frequently shows increasing degrees

of sagittal plane anterolisthesis, both in degenerative spondylolisthesis and in some cases of spondylolytic spondylolisthesis.[40]

Upright extension kMRI tends to show greater degrees of central canal and neural foramen stenosis, while flexion kMRI reveals a lessening or complete resolution of the same central canal and neural foramen narrowing (Figures 5 and 6). These phenomena were only observed at levels of disc degeneration (both disc desiccation and disc space narrowing).[41,42] In exceptional cases, de novo posterior disc herniations were revealed only on upright-extension kMRI (Figure 2). When present in the cervical spine, such cases invariably showed compression of the underlying spinal cord. Overall, this was felt to be one of the most important observations noted in this study. Interestingly, some of the posterior disc herniations became less severe when upright flexion kMRI was performed (Figure 4). This would seem to be worthy of preoperative note to those surgeons who operate on the spine in positions of flexion. Presumably this phenomenon is caused by a
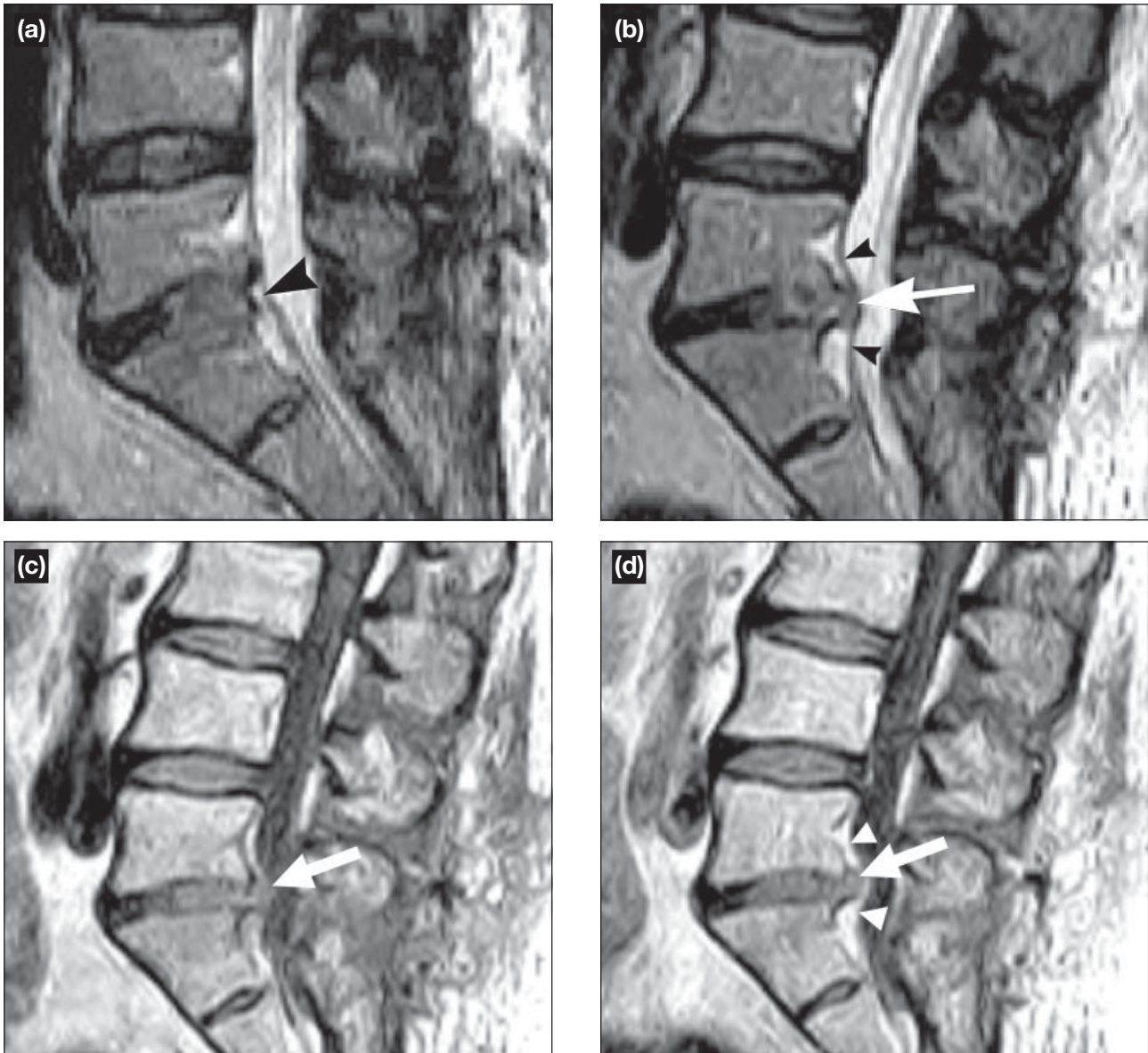
Figure 10. Postoperative fluid disc herniation 8 months following partial right-sided discectomy. (a) Recumbent mid-line sagittal T2-weighted fast spin echo magnetic resonance image (rMRI) shows a flat posterior surface (arrow) of the L5-S1 intervertebral disc. (b) Upright-neutral mid-line sagittal T2-weighted fast spin echo magnetic resonance image (pMRI) reveals a focal posterior disc herniation extending from the L5-S1 intervertebral disc space. Note the tenting of the posterior longitudinal ligament and the thecal sac (arrowheads) secondary to the mass effect of the epidural disc herniation. (c) Upright-neutral mid-line sagittal T1-weighted fast spin echo magnetic resonance image (pMRI) shows a poorly defined mass (arrow) extending posteriorly from the L5-S1 disc space. (d) Upright-neutral mid-line sagittal T1-weighted fast spin echo MRI (pMRI) following the intravenous administration of gadolinium demonstrates peripheral rim enhancement surrounding the centrally non-enhancing recurrent disc herniation (arrow). Also note the tenting of the posterior longitudinal ligament and dura mater (arrowheads) secondary to the mass effect of the epidural disc herniation. (Case provided courtesy of Dr M Rose.)

ligamentotactic effect, in that the intact fibres of the anterior and posterior longitudinal ligaments and the remaining intact peripheral posterior annular fibres have effects upon the underlying bony and soft tissues, alternately allowing more disc protrusion when lax, and less protrusion when taught. It was noted that all cases of fluctuating intervertebral disc herniation had MRI signal loss compatible with desiccation as well as intervertebral disc space height reduction.[43,44]

These disc findings were also invariably true in cases of sagittal plane hypermobile spinal instability.[45-55] It was possible to judge even minor degrees of translational hypermobile spinal instability (mobile antero- or retrolisthesis) grossly as well as by using direct region of interest measurements (Figures 5 and 7). The kMRI technique obviously does not have effects of imaging magnification and patient positioning errors potentially inherent in conventional radiographic upright
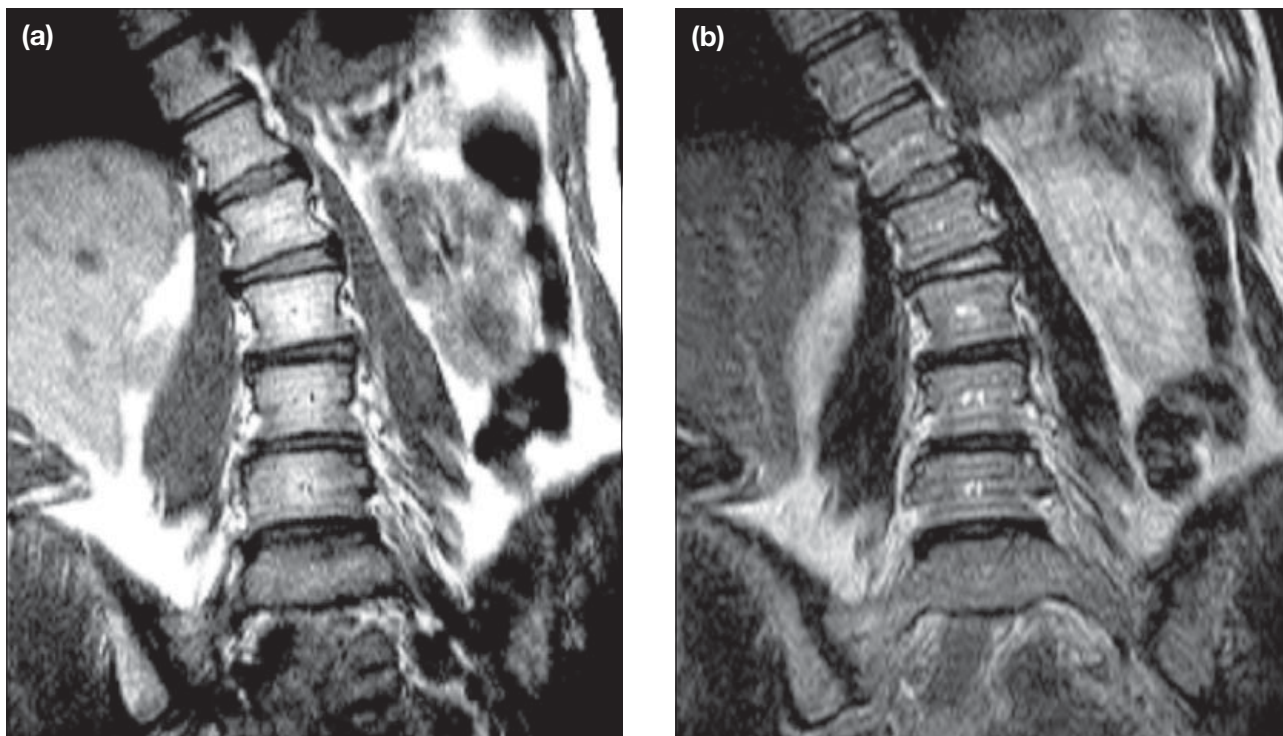
Figure 11. Lateral bending manoeuvre (example, healthy patient). (a) Standing-lateral bending coronal T1-weighted fast spin echo magnetic resonance image (kMRI) shows multilevel disc degeneration, but normal right lateral bending of the spinal column in this volunteer. There is no evidence of lateral translational dysfunctional intersegmental motion. (b) Standing-lateral bending coronal T2-weighted fast spin echo magnetic resonance image (kMRI) again shows the normal right lateral bending appearance of the spinal column.

dynamic flexion-extension studies traditionally used in these circumstances. These instances of intersegmental hypermobility seem in part to be a manifestation of spinal ligamentopathy.[56-57] As the principal roles of spinal ligaments are to stabilise the segments of the spine and also to limit the range of motion that the spinal segments can traverse, degenerative stretching or frank rupture of these ligaments will predictably allow some degree of intersegmental hypermobility.[58-63] Other alterations in the intervertebral discs and posterior spinal facet joints will have either positive (hypermobility) or negative (hypomobility) effects upon intersegmental motion.[64-67]

Also noted at levels of intersegmental degeneration (degenerated intervertebral disc, posterior spinal facet joints, spinal ligaments, intrinsic spinal muscles) was a sagittal plane hypermobile 'rocking' of the adjacent vertebrae in relationship to each other (Figures 4 and 6).[68] Observation of the opposed adjacent vertebral endplates in such cases showed them to move in relationship to each other to a much greater degree than is observed at levels with normal intervertebral discs as judged by MRI (Figures 4 and 6). This pathological movement is termed dysfunctional intersegmental motion (DIM). The significance of DIM is believed to

be in the compelling theoretical possibility that such pathologic vertebral motion may engender generalised-progressive accelerated intersegmental degeneration due to the effects of long-term repetitive micro-autotrauma. The self-protecting/stabilising spinal mechanisms inherent in the normal intervertebral discs, posterior spinal facet joints, and intact spinal ligaments/muscles are lacking in such patients, perhaps initiating a progressive degenerative cascade of degenerative autotraumatising intersegmental hypermobility.

The postoperative spine may perhaps be best analysed by p/kMRI for patients who have undergone surgical intersegmental fusion procedures.[69] In the absence of ferromagnetic fusion implants, the MRI unit was capable of identical evaluation, compared with the preoperative spine. Cases of intersegmental fusion, for example, showed no evidence of intersegmental motion, thereby confirming postoperative intersegmental stability (Figure 8). Overall mobility of the spine may also be negatively impacted by discectomy alone, unaccompanied by surgical bony fusion.[70] Other findings in the postoperative spine have included hypermobile instability between the vertebral segments above the level of a successful fusion only observed with upright, flexion imaging (Figure 9), and the revelation
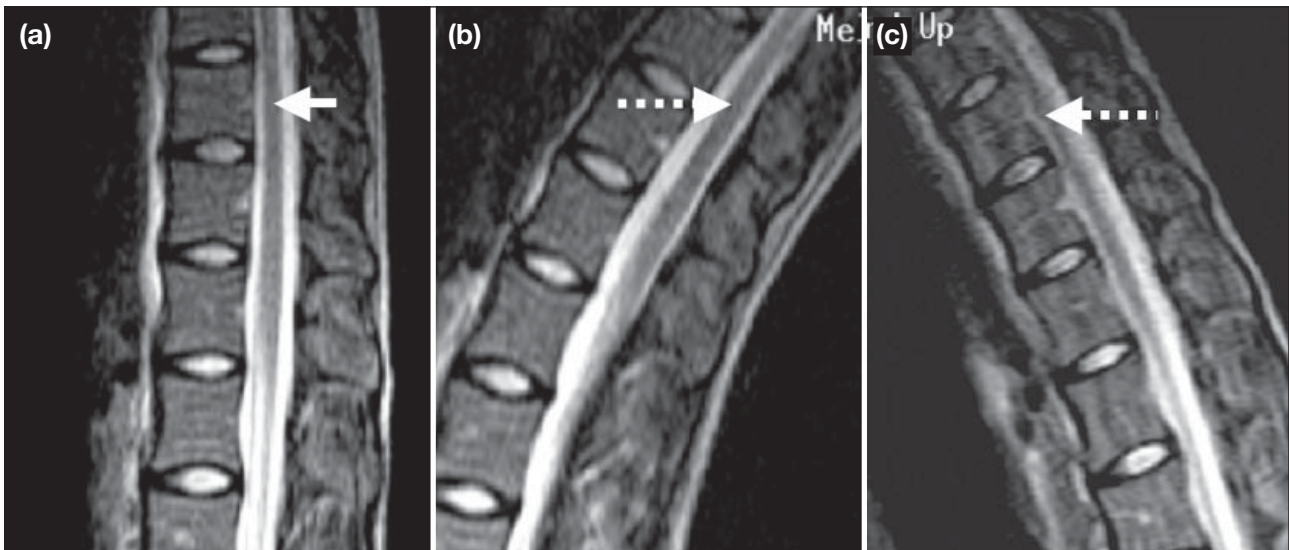
Figure 12. Spinal cord mobility analysis. (a) Recumbent mid-line sagittal T2-weighted spin echo magnetic resonance image (rMRI) shows the normal position of the spinal cord/conus medullaris (arrow). (b) Upright-extension mid-line sagittal T2-weighted spin echo MRI (kMRI) demonstrates posterior movement of the spinal cord/conus medullaris within the spinal subarachnoid space (dashed arrow). (c) Upright-flexion midline sagittal T2-weighted spin echo magnetic resonance image (kMRI) reveals anterior displacement of the spinal cord (dashed arrow). This study shows normal distal spinal cord mobility. This type of evaluation may enable the analysis of clinically suspected cases of congenital or postoperative spinal cord tethering.
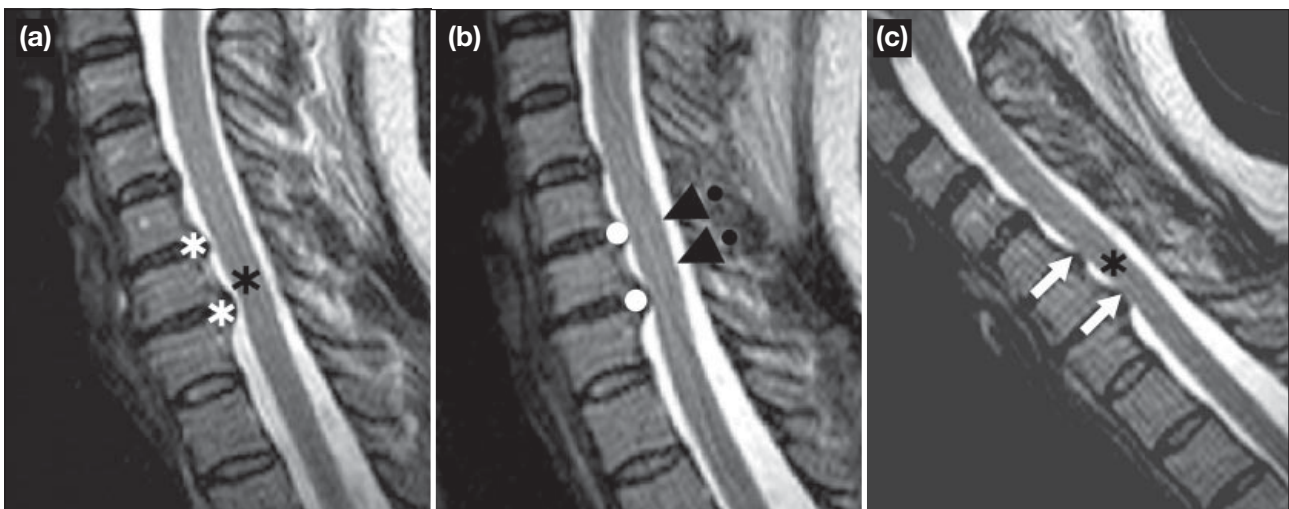

Figure 13. Provocative p/kMRI: clinical case of 'Lhermitte's Syndrome', or electrical sensations extending down both upper extremities upon maximum flexion of the cervical spine. (a) Recumbent mid-line sagittal T2-weighted spin echo magnetic resonance image (rMRI) shows the normal appearance of the cervical spinal cord (black asterisk) and the 2 level posterior disc protrusions at the C5-6 and C6-7 levels (white asterisks). (b) Upright-neutral mid-line sagittal T2-weighted spin echo magnetic resonance image (kMRI) demonstrates anterior displacement of the spinal cord (dashed arrows), now resting against the posterior disc protrusions (dots). (c) Upright-flexion mid-line sagittal T2-weighted spin echo magnetic resonance image (kMRI) reveals draping of the spinal cord (asterisk) over the 2 posterior disc protrusions (arrows). The patient only manifested symptoms consistent with Lhermitte's Syndrome during this flexion study. This study shows the potential provocative nature of dynamic-kinetic MRI (kMRI) in its ability to correlate a specific imaging acquisition with a specific clinical syndrome.

of recurrent disc herniation following prior partial discectomy only visualised with the patient in the upright position (Figure 10).

Spinal column mobility cannot only be assessed with simple flexion-extension manoeuvres. When the patient is placed in the MRI unit sideways (angled 90° right or left from frontal standing position), lateral bending movement of the spine can also be analysed (Figure 11). Spinal cord motion is another dynamic factor that may be amenable to analysis in cases where there is clinically suspected congenital or postoperative spinal cord tethering. In test cases, for example, the conus medullaris was seen to freely move anteriorly and
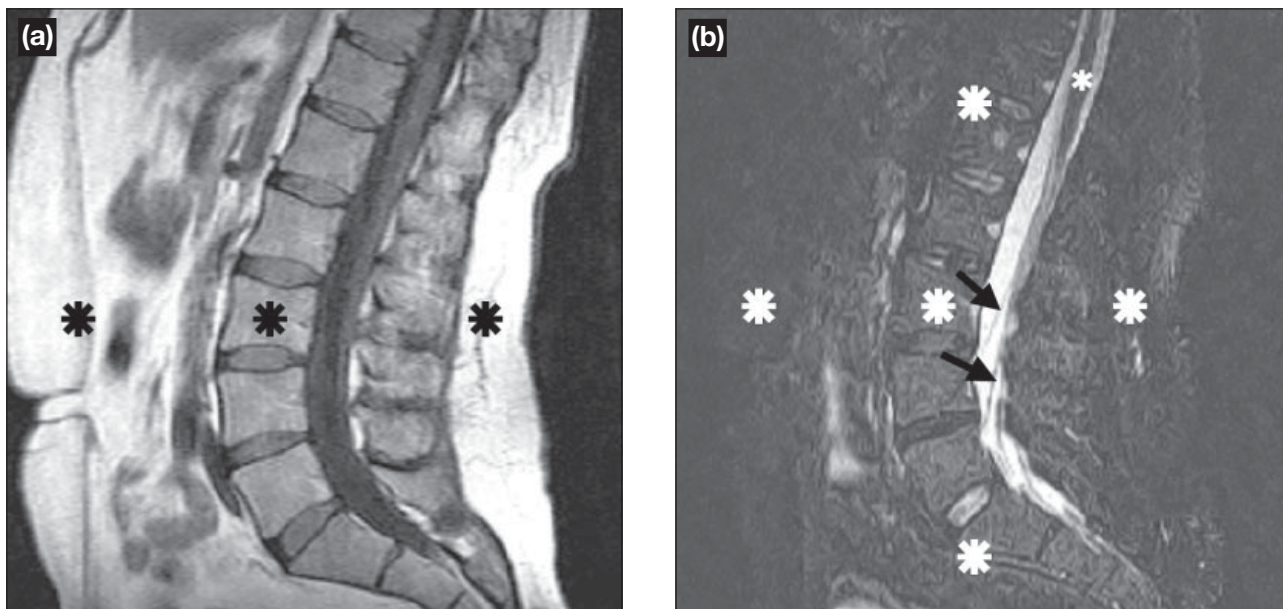
Figure 14. Fat suppression (STIR; short tau inversion recovery) technique. (a) Recumbent mid-line sagittal T1-weighted fast spin echo magnetic resonance image (rMRI) shows normal vertebral marrow, epidural, and perivertebral fat (asterisks). (b) Recumbent mid-line sagittal T2-weighted fast spin echo magnetic resonance image (rMRI) with fat suppression (STIR) shows excellent fat suppression equally across the entire image (large asterisks). Note the good visualization of the conus medullaris (small asterisk) and the nerve roots of the cauda equina (arrows).

posteriorly on flexion and extension kMRI, respectively (Figure 12).

Provocative p/kMRI is an experimental technique that may be of major practical relevance in the future. By comparing images where the patient is pain or symptom-free, with a specific position in which the patient experiences pain or symptom(s), the imaging specialist may be able to clearly link the medical images with the clinical syndrome. In this manner, provocative p/kMRI may become a truly specific diagnostic imaging method for patients with spinal disease (Figure 13).

The images of the cervical and lumbar spine suffered very little from motion artifacts from either cerebrospinal fluid (CSF) or body origin — no study was degraded to the point of being uninterpretable. Patient motion was not a problem, this being overcome by simply placing the scan table at 5° posterior tilt enabling the patient to passively rest against the table during the MRI acquisitions. In addition, it was found to be unnecessary to stand the patient for upright p/kMRI of the cervical and thoracic spines. At present, only 1 sagittal standing sequence is felt to be necessary for evaluation of the lumbar spine to analyse the lumbosacral spine for true postural curvature and for considering issues of spinal balance.[71-74] The remainder of the lumbosacral spine p/kMRI examination may be performed in the sitting position.

Chemical shift artifact was minor on all images — being directly related to field strength; this effect would be expected to be less than one-half that experienced at 1.5 T. In addition, the degree of motion artifact from such sources as the heart or CSF motion was typically minor, even without 'flow compensation' overlay techniques that were not used. This source of artifact is also related to field strength, commonly being worse on high-field MRI units.

Other relevant overlay techniques are possible on this p/kMRI unit. Included among these are fat suppression imaging (short tau inversion recovery) coupled with fast spin echo acquisitions (Figure 14). This is felt to be useful in the evaluation of spinal inflammation and spinal neoplasia.

Finally, for the patient with a possible critical stenosis of the spine in association with hypermobile instability or positional worsening of the narrowing of the central spinal canal, long time period acquisition sequences are of concern for the patient who may have greater degrees of spinal cord or cauda equina compression in upright flexion-extension p/kMRI. For this purpose, very fast acquisition sequences have been implemented in order to screen for such critical abnormalities before going forward with longer time period imaging studies (~4 to 5 minutes). Driven-equilibrium fast spin echo acquisitions offer excellent quality imaging in a
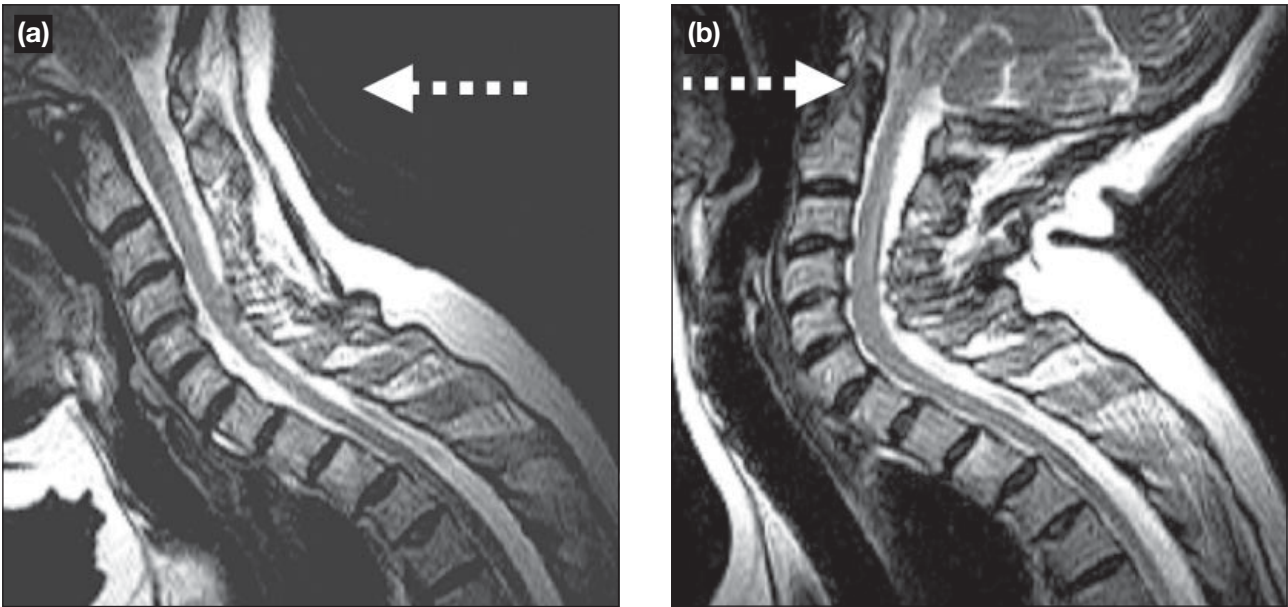
Figure 15. Ultra-fast imaging techniques for application with spinal stress manoeuvres: kMRI. (a) Upright-flexion (arrow) mid-line sagittal T2-weighted driven-equilibrium magnetic resonance image (kMRI) demonstrates normal spinal column mobility (17 seconds x 2 NEX = 34 seconds). (b) Upright-extension (arrow) mid-line sagittal T2-weighted driven-equilibrium magnetic resonance image (kMRI) again shows normal spinal column mobility. Note that there is some increase in the posterior disc protrusions at multiple levels, increased infolding of the posterior spinal ligamentous structures, and consonant minor, non-compressive narrowing of the anteroposterior dimension of the spinal canal (17 seconds x 2 NEX = 34 seconds). These single-slice, driven-equilibrium images each required approximately fifteen seconds to acquire. This technique will likely prove to be important for patients with critical stenosis of the central spinal canal under conditions of hypermobile instability, where the spinal cord may be in danger of compression during stress manoeuvres. The driven equilibrium sequences should allow very brief imaging acquisitions and enable dynamic-kinetic patient positions to be safely assumed for very short periods of time required by this technique.
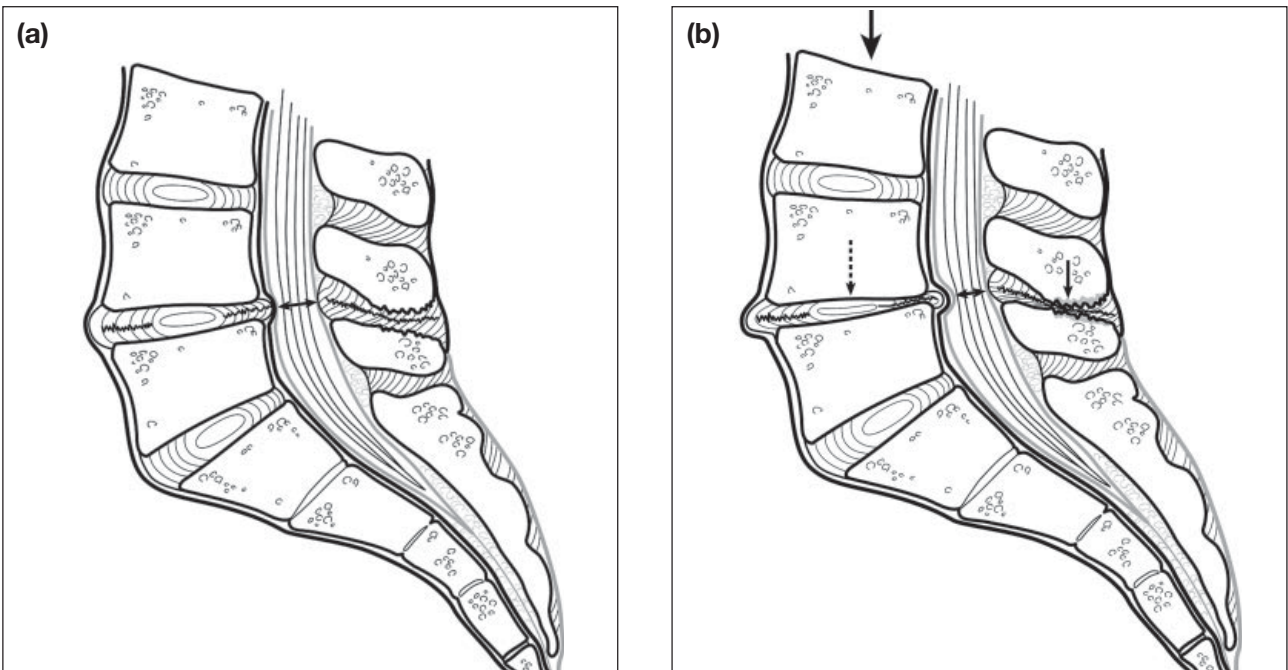

Figure 16. Telescoping of the spinal column associated with degenerative disc disease. (a) Diagram of recumbent spine showing degenerative disc disease at the L4-5 level (anterior serrated lines), and degeneration of the interspinous ligament at this same level (posterior serrated line). Note the bulging of the degenerated intervertebral disc at L4-5 resulting in mild narrowing of the central spinal canal (double-headed arrow). (b) Diagram of the upright-neutral lumbosacral spine demonstrating gravity-related (large solid arrow) narrowing of the L4-5 intervertebral disc space (dashed arrow) and interspinous space (small solid arrow) compared with the recumbent image in Figure 16a, together with redundancy of the soft tissues bordering on the central spinal canal. This telescoping of the spinal column may result in varying degrees of worsening stenosis of the central spinal canal (double-headed arrow).
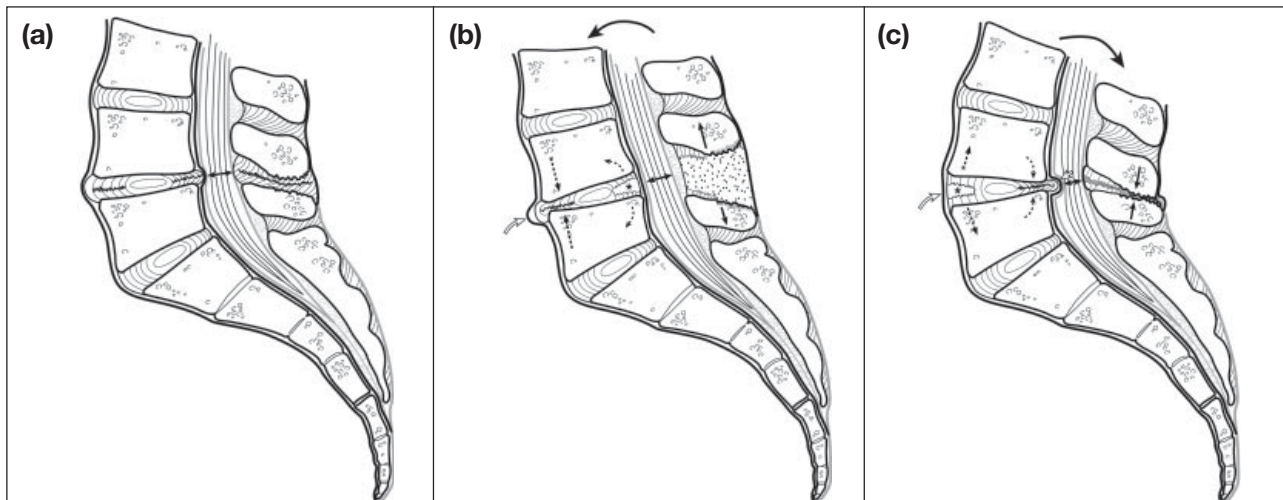
Figure 17. Ligamentotactic and ligamentopathic effects. (a) Diagram of the recumbent spine showing degeneration of the L4-5 inter-vertebral disc and interspinous ligament (serrated lines). Note the mild peripheral bulging of the intervertebral disc at L4-5, and the minor narrowing of the central spinal canal (double-headed arrow). Also note the near parallel position of the intervertebral end plates on either side of the L4-5 disc. (b) Diagram of the upright-flexed (solid curved arrow) lumbosacral spine shows an increase in the anterior disc protrusion (open curved arrow) related to laxity of the anterior longitudinal ligament and anterior fibres of the annulus fibrosus, lessening of the posterior disc protrusion/bulge caused by tension of the posterior longitudinal ligament and remaining intact posterior fibres of the annulus fibrosus, splaying of the spinous processes (solid straight arrows), hyperexpansion of the interspinous space (stippling), opening up of the posterior aspect of the disc space (asterisk, dashed curved arrows), and narrowing of the anterior aspect of the disc space (straight dashed arrows). Note that the central spinal canal becomes wider (double-headed arrow) compared with the neutral position or extension manoeuvre (Figures 17a and 17c). Also note that the opposed vertebral endplates on either side of the degenerated L4-5 intervertebral disc assume an anteriorly directed wedge configuration (dysfunctional intersegmental motion; see Figure 17c). (c) Diagram of the upright-extended lumbosacral spine shows an increase in the posterior disc protrusion (open straight arrow) related to laxity of the posterior longitudinal ligament and anterior fibres of the annulus fibrosus, lessening of the anterior disc protrusion caused by tension of the anterior longitudinal ligament and remaining intact anterior fibres of the annulus fibrosus, collision of the spinous processes (solid straight arrows), opening up of the anterior disc space (asterisk, dashed straight arrows), and narrowing of the posterior aspect of the disc space (dashed curved arrows). Note that the central spinal canal becomes narrower (double-headed arrow) compared with the neutral position or flexion maneuver (Figures 17a and 17b). Also note that the opposed vertebral endplates on either side of the degenerated L4-5 intervertebral disc assume a posteriorly directed wedge configuration. This latter observation indicates dysfunctional intersegmental motion at this level of disc degeneration, a result in part of intersegmental ligamentopathy (ligamentous laxity/rupture).
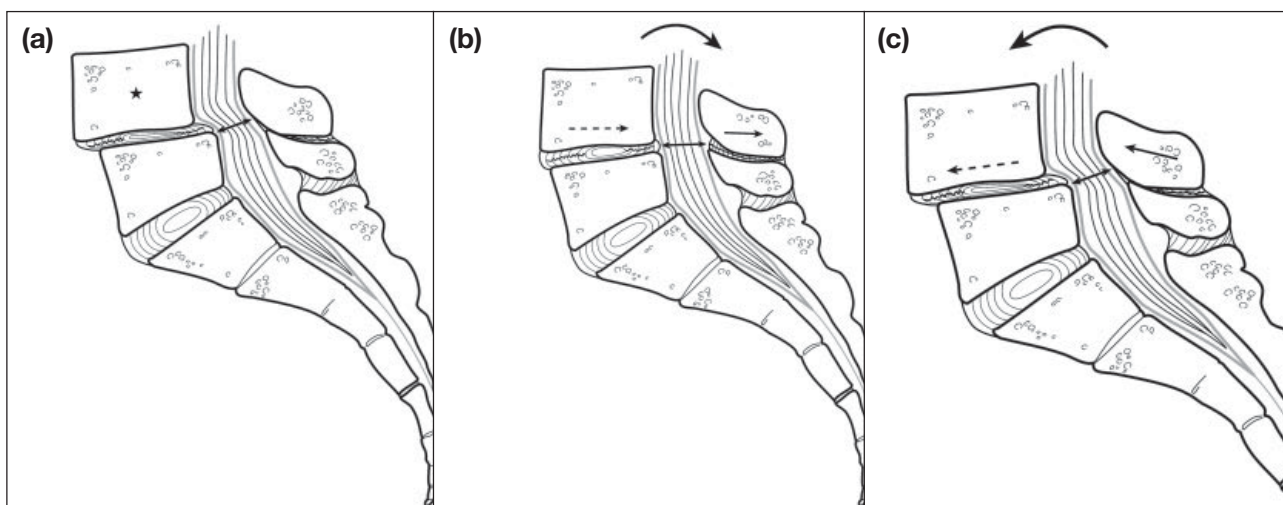

Figure 18. Translational hypermobile instability associated with dynamic flexion-extension imaging (kMRI). (a) Diagram of the recumbent spine showing degeneration of the L4-5 intervertebral disc and interspinous ligament (serrated lines), and degenerative anterior spondylo-listhesis of L4 (star) on L5. Note the minor narrowing of the central spinal canal (double-headed arrow). (b) Diagram of the upright-extended (solid curved arrow) lumbosacral spine shows a partial reduction of the spondylolisthesis (dashed and solid straight arrows). Note that the central spinal canal becomes wider (double-headed arrow) compared with the neutral or flexion diagrams (Figures 18a and 18c). (c) Diagram of the upright-flexed lumbosacral spine (solid curved arrow) reveals a minor increase in the anterior translational spondylolisthesis (dashed and solid straight arrows). Note that the central spinal canal becomes narrower (double-headed arrow) compared with the neutral or extension diagrams (Figures 18a and b).
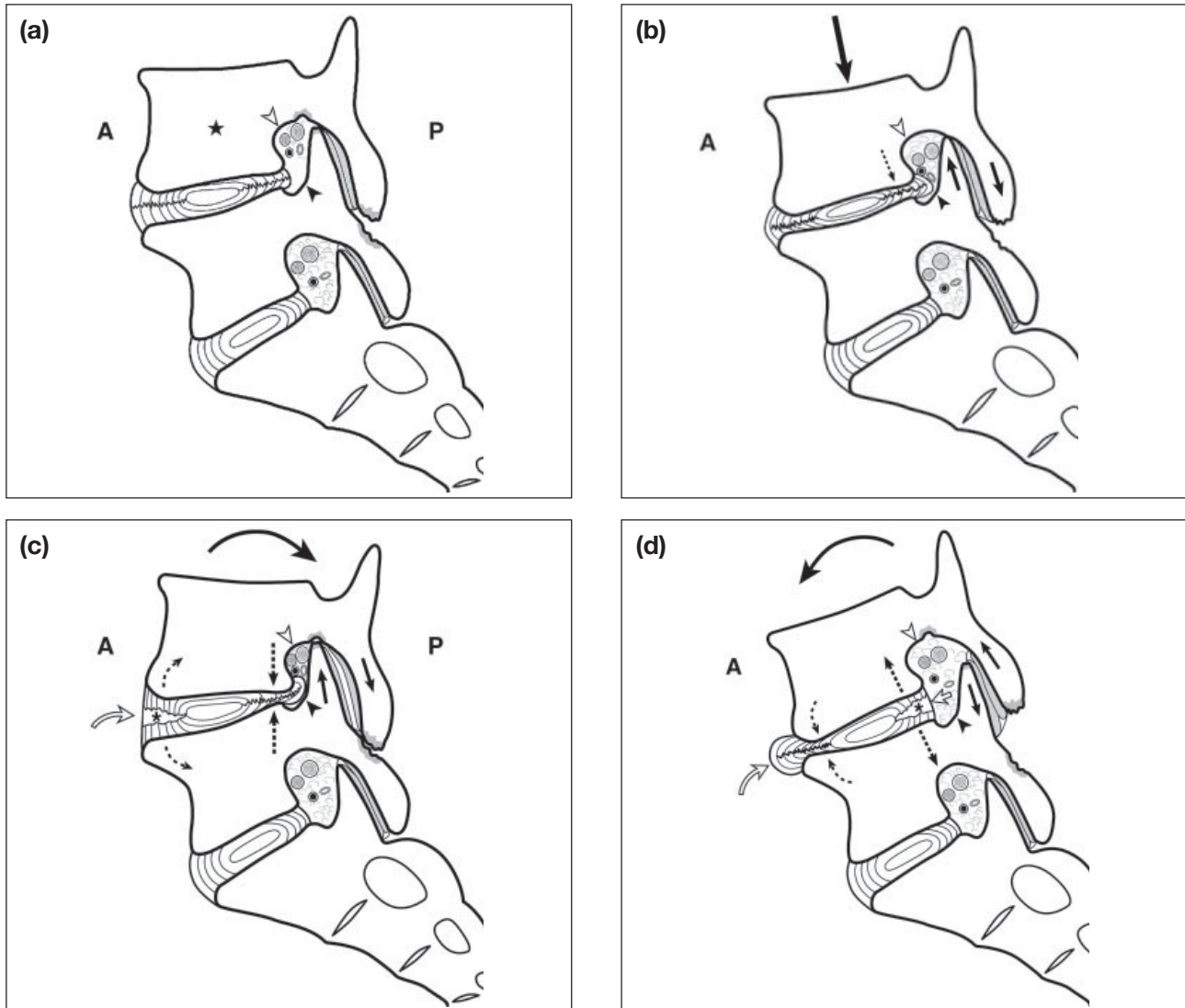
Figure 19. Effects of weight bearing-neutral posture (upright-neutral gravity and muscular balance effects), and dynamic-kinetic manoeuvres on the neural foramina; dysfunctional intersegmental motion (DIM) at levels of disc degeneration. (a) Diagram of the recumbent spine showing degeneration of the L4-5 intervertebral disc (serrated lines). Note the minor narrowing of the neural foramen at this level (open arrowhead). The inferior recess of the neural foramen remains open (solid arrowhead). Also note the near parallel position of the intervertebral end plates on either side of the L4-5 disc. (b) Diagram of the upright-neutral spine (large solid straight arrow; standing postural axial loading) showing degeneration of the L4-5 intervertebral disc (serrated lines). Note the minor increase in narrowing of the neural foramen at this level (open arrowhead; compared with Figure 19a). The inferior recess of the neural foramen is further narrowed (solid arrowhead) by the increasing protrusion of the posterolateral aspect of the intervertebral disc (dashed arrow; compared with Figure 19a). Also note the minor reduction in superoinferior height of the bony margins of the neural foramen, in part as a result of the disc space narrowing (dashed arrow) associated with subluxation of the spinal facet joint articular processes (small straight solid arrows). (c) Diagram of the upright-extended (curved solid arrow) lumbosacral spine shows, an increase in the posterior disc protrusion/bulge, and narrowing of the posterior aspect of the disc space (straight dashed arrows). Note the increasing posterior disc protrusion associated with obliteration of the inferior recess (solid arrowhead) and superior recess (open arrowhead) of the neural foramen (solid arrowhead), the opening up of the anterior disc space (asterisk, dashed curved arrows), the narrowing of the posterior aspect of the disc space (straight dashed arrows), the partial shearing contracting subluxation of the posterior spinal facet (zygapophyseal) joint processes (solid straight arrows), and the diminution in size of the anteriorly bulging disc (open curved arrow). Also note that the opposed vertebral endplates on either side of the degenerated L4-5 intervertebral disc assume a posteriorly directed wedge configuration (dysfunctional intersegmental motion). (d) Diagram of the upright-flexed (solid curved arrow) lumbosacral spine demonstrating anterior disc protrusion (open curved arrow) related to laxity of the anterior longitudinal ligament, lessening of the posterior disc protrusion/bulge as a result of tension of the remaining intact posterior annular fibers, opening up of the posterior aspect of the disc space (asterisk, straight dashed arrows), narrowing of the anterior aspect of the disc space (curved dashed arrows), the partial shearing distracting subluxation of the posterior spinal facet (zygapophyseal) joint processes (solid straight arrows), and the opening up of the superior recess (open arrowhead) and inferior recess (solid arrowhead) of the spinal neural foramen. Also note that the opposed vertebral endplates on either side of the degenerated L4-5 intervertebral disc assume an anteriorly directed wedge configuration. This latter observation indicates dysfunctional intersegmental motion at this level of disc degeneration, a result in part of intersegmental ligamentopathy (ligamentous laxity/rupture).

Table 9. Combined effects of spinal degeneration with telescoping, diskopathy, ligamentopathy, hypermobile instability, and dysfunctional intersegmental motion.

- Spinal stenosis (central spinal canal, lateral recesses [subarticular zone], neural foramina)
- Spinal cord/nerve compression
- Somatic nerve ending irritation
- Neuromuscular/ligamentous autotrauma
- Related patient signs/symptoms

Table 10. Clinicoradiological relevance of p/kMRI.

Patient care considerations
- Improvement of imaging sensitivity over that of recumbent examinations

Medicolegal aspects
- Revelation of diagnoses missed or underestimated on recumbent examinations

Workers' compensation
- Revelation of occult pathology not found on recumbent examinations

Economic factors

fraction of the time (~17 seconds x 2 NEX = 34 seconds) required for traditional sequences, and allow safe imaging of almost any patient with p/kMRI (Figure 15). These fast high-resolution techniques may be a major if not sole method of imaging the spine using p/kMRI in the future.

CONCLUSIONS

To conclude, the potential relative beneficial aspects of upright, weight-bearing MRI and dynamic-kinetic MRI spinal imaging on this system over that of recumbent MRI include clarification of true sagittal upright neutral spinal curvature unaffected by patient positioning, revelation of occult degenerative spinal disease dependent on true axial loading (weight-bearing) [Figure 16], unmasking of kinetic-dependent degenerative spinal disease (flexion-extension) [Figures 17, 18, and 19], and the potential ability to scan the patient in the position of clinically relevant signs and symptoms (Figure 13, Table 9). Scanning the patient in the operative position, enabling the surgeon to have a true preoperative picture of the intraoperative pathologic morphology, is a topic currently under investigation.[75] This MRI unit also demonstrated low claustrophobic potential and yielded high-resolution images with little motion/chemical/magnetic susceptibility artifact.

Based on initial non-statistical clinical experience with this unit, it is felt that mid-field MRI may prove to be the optimal field strength for routine, anatomic MRI of the spinal column in degenerative as well as other spinal disease categories.[76] In addition, the evidence thus far indicates that p/kMRI may prove to be efficacious to incorporate as a part of the clinical diagnosis-treatment paradigm for patients with spinal, radicular, and referred pain syndromes originating from spinal pathology (Table 10). Simply stated, rMRI underestimates the maximum degree of degenerative spinal pathology and misses altogether its dynamic nature, factors that are optimally revealed on p/kMRI.

REFERENCES

1. Jinkins JR. Atlas of neuroradiologic embryology, anatomy and variants. Philadelphia: Lippincott-Williams and Wilkins; 2000.
2. Jinkins JR, Green C, Damadian R. Upright, weight-bearing, dynamic-kinetic MRI of the spine: pMRI/kMRI. Rivista di Neuroradiol 2001;14:135:2001.
3. Smith TJ, Fernie GR. Functional biomechanics of the spine. Spine 1991;16:1197-1203.
4. Smith TJ. In vitro spinal biomechanics: experimental methods and apparatus. Spine 1991;16:1204-1210.
5. Marras WS, Granata KP. A biomechanical assessment and model of axial twisting in the thoracolumbar spine. Spine 1995;20:1440-1451.
6. Resnick DK, Weller SJ, Benzel EC. Biomechanics of the thoracolumbar spine. Neurosurg Clin N Am 1997;8:455-469.
7. Berne D, Goubier JN, Lemoine J, et al. The aging of the spine. Eur J Orthop Surg Traumatol 1999;9:125-133.
8. Boden SD, Wiesel SW. Lumbosacral segmental motion in normal individuals: have we been measuring instability properly? Spine 1990;15:571-576.
9. Danielson BI, Willén J, Gaulitz A, et al. Axial loading of the spine during CT and MR in patients with suspected lumbar spinal stenosis. Acta Radiol 1998;39:604-611.
10. Frymoyer JW, Frymoyer WW, Wilder DG, et al. The mechanical and kinematic analysis of the lumbar spine in normal living human subjects in vivo. J Biomech 1979;12:165-172.
11. Hedman TP, Fernie GR. In vivo measurement of lumbar spinal creep in two seated postures using magnetic resonance imaging. Spine 1995;20:178-183.
12. Hilton RC, Ball J, Benn RT. In-vitro mobility of the lumbar spine. Annals Rheum Dis 1975;38:378-383.
13. Inufusa A, An HS, Lim T-H, et al. Anatomic changes of the spinal canal and intervertebral foramen associated with flexion-extension movement. Spine 1996;21:2412-2420.
14. Mayoux-Benhamou MA, Revel M, Aaron C, et al. A morphometric study of the lumbar foramen: influence of flexion-extension movements and of isolated disc collapse. Surg Radiol Anat 1989;11:97-102.
15. Nachemson AL, Schultz AB, Berkson MH. Mechanical properties of human lumbar spine motion segments: influences of age, sex, disc level, and degeneration. Spine 1979;4:1-8.
16. Nowicki BH, Haughton VM, Schmidt TA, et al. Occult lumbar lateral spinal stenosis in neural foramina subjected to physiologic loading. AJNR 1996;17:1605-1614.
17. Pennal GF, Conn GS, McDonald G, et al. Motion studies of the lumbar spine: a preliminary report. J Bone Joint Surg 1972;54B:442-452.
18. Penning L, Wilmink JT. Posture-dependent bilateral compression of l4 or l5 nerve roots in facet hypertrophy: a dynamic CT-myelographic study. Spine 1987;12:488-500.
19. Schönström N, Lindahl S, Willén J, et al. Dynamic changes in the dimensions of the lumbar spinal canal: an experimental study in vitro. J Orthop Res 1989;7:115-121.

20. Sortland O, Magnes B, Hauge T. Functional myelography with metrizamide in the diagnosis of lumbar spinal stenosis. Acta Radio 1977;355(Suppl):42-54.
21. White AS, Panjabi MM. The basic kinematics of the human spine: a review of past and current knowledge. Spine 1978;3: 12-29.
22. Willén J, Danielson B, Gaulitz A, et al. dynamic effects on the lumbar spinal canal: axially loaded CT-myelography and MRI in patients with sciatica and/or neurogenic claudication. Spine 1997;22:2968-2976.
23. Wilmink JT, Penning L, van den Burg W. Role of stenosis of spinal canal in L4-L5 nerve root compression assessed by flexion-extension myelography. Neuroradiology 1984;26: 173-181.
24. Friberg O. Lumbar instability: a dynamic approach by traction — compression radiography. Spine 1987;12:119-120.
25. Fujiwara A, An HS, Lim TH, et al. Morphologic changes in the lumbar intervertebral foramen due to flexion-extension, lateral bending, and axial rotation: an in vitro anatomic and biomechanical study. Spine 2001;26:876-882.
26. Hayes MA, Howard TC, Gruel CR, et al. Roentgenographic evaluation of lumbar spine flexion-extension in asymptomatic individuals. Spine 1989;14:327-331.
27. Lee RR, Abraham RA, Quinn CB. Dynamic physiologic changes in lumbar CSF volume quantitatively measured by three-dimensional fast spin-echo MRI. Spine 2001;26:1172-1178.
28. Panjabi MM, Takata K, Goel VK. Kinematics of lumbar intervertebral foramen. Spine 1983;8:348-357.
29. Pearcy MJ, Tibrewal SB. Axial rotation and lateral bending in the normal lumbar spine measured by three-dimensional radiography. Spine 1984;9:582-587.
30. Penning L, Wilmink JT. Biomechanics of lumbosacral dural sac. a study of flexion-extension myelography. Spine 1981;6: 398-408.
31. Revel M, Mayoux-Benhamou MA, Aaron C, et al. Morphological variations of the lumbar foramina. Rev Rhum Mal Osteoartic 1988;55:361-366.
32. Stokes IA, Frymoyer JW. Segmental motion and instability. Spine 1987;12:688-691.
33. Stokes IA, Wilder DG, Frymoyer JW, et al. Assessment of patients with low-back pain by biplanar radiographic measurement of intervertebral motion. Spine 1981;6:233-240.
34. Takayanagi K, Takahashi K, Yamagata M, et al. Using cineradiography for continuous dynamic-motion analysis of the lumbar spine. Spine 2001;26:1858-1865.
35. Wildermuth S, Zanetti M, Duewell S, et al. Lumbar spine: quantitative and qualitative assessment of positional (upright flexion and extension) MR imaging and myelography. Radiology 1998; 207:391-398.
36. Wisleder D, Smith MB, Mosher TJ, et al. Lumbar spine mechanical response to axial compression load in vivo. Spine 2001; 26:E403-E409.
37. Wisleder D, Werner SL, Kraemer WJ, et al. A method to study lumbar spine response to axial compression during magnetic resonance imaging. Spine 2001;26:E416-E420.
38. Zamani AA, Moriarty T, Hsu L, et al. Functional MRI of the lumbar spine in erect position in a superconducting open-configuration MR system: preliminary results. JMRI 1998;8:1329-1333.
39. Leviseth G, Drerup B. Spinal shrinkage during work in a sitting posture compared to work in a standing posture. Clin Biomech 1997;12:409-418.
40. Lowe RW, Hayes TD, Kaye J, et al. standing roentgenograms in spondylolisthesis. Clin Orthop 1976;117:80-84.
41. Devor M, Rappaport ZH. Relation of foraminal (lateral) stenosis to radicular pain. AJNR 1996;17:1615-1617.
42. Hasegawa T, An HS, Haughton VM, et al. Lumbar foraminal stenosis: critical heights of the intervertebral discs and foramina. J Bone Joint Surg 1995;77-A:32-38.
43. Pfirrmann CWA, Metzdorf A, Zanetti M. Magnetic resonance classification of lumbar intervertebral disc degeneration. Spine 2001;26:1873-1878.
44. Shiwei Y, Haughton VM, Sether LA. Criteria for classifying normal and degenerated lumbar intervertebral disks. Neuroradiology 1989;170:523-526.
45. Axelsson P, Johnson R, Strömqvist B. Is there increased intervertebral mobility in isthmic adult spondylolisthesis? a matched comparative study using roentgen stereophotogrammetry. Spine 2000;25:1701-1703.
46. Boden SD, Frymoyer JW. Segmental instability: overview and classification. In: Frymoyer JW, editor. The adult spine: principles and practice. Philadelphia: Lippincott-Raven; 1997: 2137-2155.
47. Dupuis PR, Yong-Hing K, Cassidy JD, et al. Radiologic diagnosis of degenerative lumbar spinal instability. Spine 1985;10: 262-276.
48. Frymoyer JW, Selby DK. Segmental instability: rationale for treatment. Spine 1985;10:280-286.
49. Fujiwara A, Lim T-H, An HS, et al. The effect of disc degeneration and facet joint osteoarthritis on the segmental flexibility of the lumbar spine. Spine 2000;25:3036-3044.
50. Pearcy M, Shepherd J. Is there instability in spondylolisthesis? Spine 1985;10:175-177.
51. Ito M, Tadano S, Kaneda K. A biomechanical definition of spinal segmental instability taking personal and disc level differences into account. Spine 1993;18:2295-2304.
52. Pope MH, Panjabi M. Biomechanical definitions of spinal instability. Spine 1985;10:255-256.
53. Sato H, Kikuchi S. The natural history of radiographic instability of the lumbar spine. Spine 1993;18:2075-2079.
54. Posner I, White AA, Edwards WT, et al. A biomechanical analysis of the clinical stability of the lumbar and lumbosacral spine. Spine 1982;7:374-389.
55. Wood KB, Popp CA, Transfeldt EE, et al. Radiographic evaluation of instability in spondylolisthesis. Spine 1994;7:1697-1703.
56. Yahia H, Drouin G, Maurais G, et al. Degeneration of the human lumbar spine ligaments. an ultrastructural study. Path Res Pract 1989;184:369-375.
57. Fujiwara A, Tamai K, An HS, et al. The interspinous ligament of the lumbar spine: magnetic resonance images and their clinical significance. Spine 2000;25:358-363.
58. Adams MA, Hutton WC, Stott JRR. The resistance to flexion of the lumbar intervertebral joint. Spine 1980;5:245-253.
59. Dumas GA, Beaudoin L, Drouin G. In situ mechanical behavior of posterior spinal ligaments in the lumbar region. an in vitro study. J Biomechanics 1987;20:301-310.
60. Hukins DWL, Kirby MC, Sikoryn TA, et al. Comparison of structure, mechanical properties, and functions of lumbar spinal ligaments. Spine 1990;15:787-795.
61. Panjabi MM. The stabilizing system of the spine. part 1. function, dysfunction, adaptation, and enhancement. J Spinal Disorders 1992;5:383-389.
62. Panjabi MM, Goel VK, Takata K. Physiologic strains in the lumbar spinal ligaments: an in vitro biomechanical study. Spine 1982;7:192-203.

63. Sharma M, Langrana NA, Rodriguez J. Role of ligaments and facets in lumbar spinal stability. Spine 1995;20:887-900.
64. Fujiwara A, Lim TH, An HS. The effect of disc degeneration and facet joint osteoarthritis on the segemental flexibility of the lumbar spine. Spine 2000;25:3036-3044.
65. Haughton VM, Schmidt TA, Keele K, et al. Flexibility of lumbar spinal motion segments correlated to type of tears in the annulus fibrosis. J Neurosurg 2000;92:81-86.
66. Thompson RE, Pearcy MJ, Downing KJW, et al. Disc lesions and the mechanics of the intervertebral joint complex. Spine 2000;25:3026-3035.
67. Twomey LT, Taylor JR. Sagittal movements of the human lumbar vertebral column: a quantitative study of the role of the posterior vertebral elements. Arch Phys Med Rehabil 1983;64: 322-325.
68. Cartolari R, Argento G, Cardello M, et al. Axial loaded computed tomography (AL-CT) and cine AL-CT. Rivista di Neuroradiol 1998;11:275-286.
69. Jinkins JR. Posttherapeutic neurodiagnostic imaging. Jinkins JR, editor. Philadelphia: Lippincott-Raven; 1997.
70. Keller TS, Hansson TH, Holm SH, et al. in vivo creep behavior of the normal and degenerated porcine intervertebral disk: a preliminary report. J Spinal Disorders 1989;1:267-278.
71. Jackson RP, Hales C. Congruent spinopelvic alignment on standing lateral radiographs of adult volunteers. Spine 2000; 25:2808-2815.
72. Lee C-S, Lee C-K, Kim Y-T, et al. Dynamic sagittal imbalance of the spine in degenerative flat back. Spine 2001;26:2029-2035.
73. Jackson RP, Kanemura T, Kawakami N, et al. Lumbopelvic lordosis and pelvic balance on repeated standing lateral radiographs of adult volunteers and untreated patients with constant low back pain. Spine 2000;25:575-586.
74. Jackson RP, Peterson MD, McManus AC, et al. Compensatory spinopelvic balance over the hip axis and better reliability in measuring lordosis to the pelvic radius on standing lateral radiographs of adult volunteers and patients. Spine 1998;23:1750-1767.
75. Stephens GC, Yoo JU, Wilbur G. comparison of lumbar sagittal alignment produced by different operative positions. Spine 1996;21:1802-1807.
76. Jinkins JR. Acquired degenerative changes of the intervertebral segments at and suprajacent to the lumbosacral junction: a radioanatomic analysis of the nondiskal structures of the spinal column and perispinal soft tissues. Radiol Clin North Am 2001; 39:73-99.